Biophysical Chemistry 153 (2011) 126–153

Contents lists available at ScienceDirect

Biophysical Chemistry

journal homepage: http://www.elsevier.com/locate/biophyschem

Review

Gastropod nacre: Structure, properties and growth — Biological, chemical and physical basics

Fabian Heinemann [a,1], Malte Launspach [a,1], Katharina Gries [a,b], Monika Fritz [a,*]

[a] Biophysics Institute, University of Bremen, Otto-Hahn-Allee, 28359 Bremen, Germany
[b] Solid State Physics Institute, University of Bremen, Otto-Hahn-Allee, 28359 Bremen, Germany

ARTICLE INFO

Article history:
Received 3 September 2010
Received in revised form 8 November 2010
Accepted 8 November 2010
Available online 19 November 2010

Keywords:
Biogenic composite
Biomineralising proteins
Columnar nacre
Mechanical properties
Biomineralisation
Organic matrix

ABSTRACT

The biogenic polymer/mineral composite nacre is a non-brittle biological ceramic, which self-organises in aqueous environment and under ambient conditions. It is therefore an important model for new sustainable materials. Its highly controlled structural organization of mineral and organic components at all scales down to the nano - and molecular scales is guided by organic molecules. These molecules then get incorporated into the material to be responsible for properties like fracture mechanics, beauty and corrosion resistance. We report here on structure, properties and growth of columnar (gastropod) nacre with emphasis on the genus *Haliotis* in contrast to sheet nacre of many *bivalves*.

Contents

* Corresponding author. Tel.: +49 421 21862281; fax: +49 421 2182974.
E-mail address: mf@biophysik.uni-bremen.de (M. Fritz).
[1] Both authors contributed equally to the work.

0301-4622/$ – see front matter © 2010 Elsevier B.V. All rights reserved.
doi:10.1016/j.bpc.2010.11.003

Abbreviations

SEM	scanning electron microscopy
TEM	transmission electron microscopy
AFM	atomic force microscopy
EDTA	ethylenediaminetetraacetic acid
HR-TEM	high resolution transmission electron microscopy
FIB	focused ion beam
PIPS	precision ion polishing system
EDX	energy dispersive X-ray spectroscopy
EELS	electron energy loss spectroscopy
X-PEEM	X-ray photoelectron emission spectromicroscopy
IGF	insulin growth factor
WAP	whey acidic protein
MW	molecular weight (in Da)
XANES	X-ray absorption near edge spectromicroscopy
WGA	wheat germ agglutinine
SDS-PAGE	sodium dodecylsulfate polyacrylamide gel electrophoresis
ACC	amorphous calcium carbonate
PIC	polarisation-dependant imaging contrast

Symbols

wt.%	weight percent
E	Young modulus
ε	strain
σ	stress
ρ	density
κ	aspect ratio
ν	Poisson ratio
A	area
W_{ext}	external work
W_{ela}	elastic work
G, J	energy release rate
G_c, J_c, R	critical energy release rate
a	crack length/crack extension
Φ	volume fraction
h	platelet height
γ	surface energy
τ	shear strength
G_p	shear modulus of organic phase
B	equilibrium lattice spacing of atoms
n, m	material constants

1. Introduction

600 million years ago a biogenic composite arose in ancestors of our nowadays snails and bivalves, which is still the protective structure to prevent the animals from being fed by predators. Unlike comparable man-made materials – for example, ceramics or laminated safety glass – nacre self-organises in an aqueous environment and under ambient conditions.

These biominerals produced by many organisms are characterised by high functionality and outstanding properties compared to their abiogenic counterparts. They are usually formed at ambient conditions, their components are nontoxic and they are well adapted to the circular flow of material in the living world due to evolutionary pressure. Biominerals are therefore important models for new sustainable materials. One of the best studied biomineral is the iridescent part of the shells of gastropods and bivalves — nacre (Fig. 1A).

The structure of nacre is studied since many years and early scanning and transmission electron microscopy investigations in the 60s to 80s showed already the fascinating structure of the material [1–4] (Fig. 1B) with mineral layers of a height of about 0.5 μm highly organized in up to 2000 vertical units. The material, which is formed in a self-organisation process is a composite of a small amount of organic material between these mineral layers giving the exceptional mechanical properties [5,6]. The single layers of minerals are formed by small crystals (platelets or tablets) with a diameter of 5 to 10 μm, which contact each other on either lateral boundary (Fig. 1C).

Thus it is obvious that one of the essential features of the composite nacre is its highly controlled structural organization of mineral and organic components at all scales down to the nano- and molecular-scale. The process of mineral formation can be called an "organic matrix-mediated" [7] process, where the organic material first guides the process of mineralisation by molecular recognition and interactions during growth and then gets incorporated into the material to be responsible for properties like fracture mechanics, beauty and corrosion resistance in sea water.

The material formed in a self-organised manner is a polymer/mineral composite, a non-brittle biogenic fiber-inforced ceramic and a beautiful material with rainbow colour iridescence. It is made of non-toxic components, which are highly available in nature.

The outstanding properties of this biological material have gained widespread interest between the different disciplines in science like geology, biology, chemistry, physics and materials science.

The beauty and mechanical properties of nacre are both due to the highly organised structure and the hierarchical construction. The high ratio of mineral to organic constructed in a brick and mortar like fashion leads to a seemingly contradictory combination of strength, toughness and elasticity. An account for the fracture resistance may be the strong interaction, intimate association and binding between organic and inorganic phase, which shows the importance of the interaction on the molecular scale.

After secretion by the epithelial cells organic molecules act in solution and as insoluble organic template on the polymorph selection, structure and morphology of the aragonite inorganic crystals. The importance of electrostatic binding or association and geometric epitaxis between biological molecules and inorganic ions and/or surfaces is evident.

Biomimetic strategies based on these principles may be important energy conserving routes for sustainable materials, because biogenic polymer/mineral composite materials are usually fabricated by

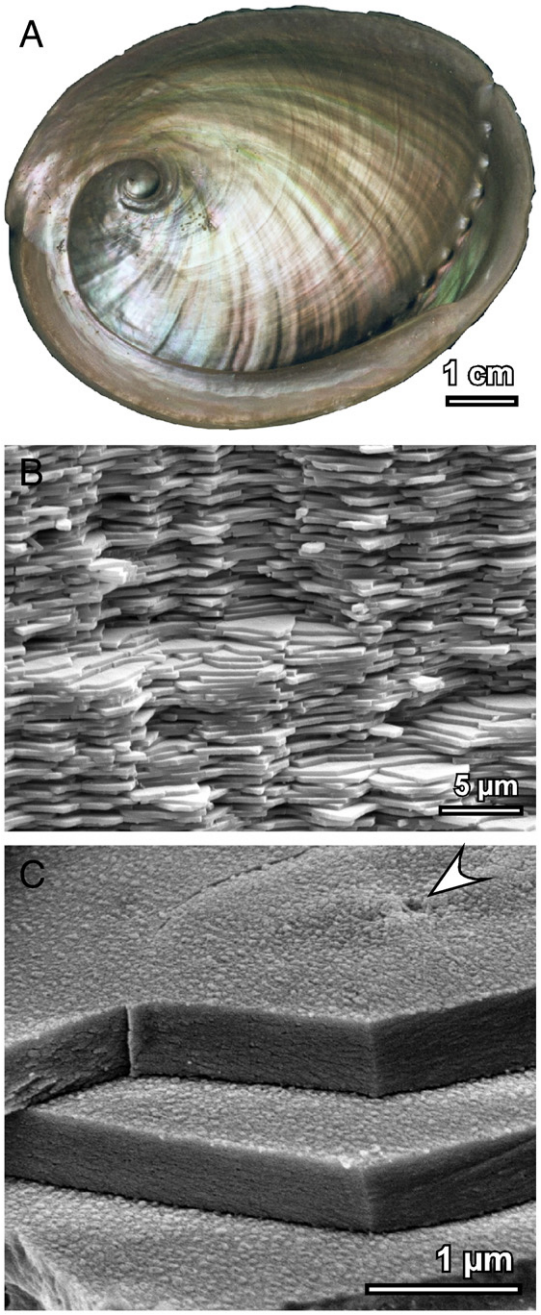

Fig. 1. Nacre of the shell of *Haliotis laevigata.* A. Photo of the inner, iridescent part of the shell. B. Scanning electron microscopy (SEM) image of a cross fracture surface of nacre. The mineral crystals are pseudohexagonal aragonite crystals (platelets or tablets) with a diameter of 5 to 10 µm and a height of about 0.5 µm, which form confluent mineral layers. The layers are highly organised and the nacreous part of a shell of a larger animal (15 to 20 cm in length) may bear up to 2000 of these vertical layers. C. Close-up view on the platelets. The surface is corrugated and there is a pronounced structure in the center (arrow).

the organisms at mild conditions like ambient temperature and pressure.

For materials science the development of new strategies in the controlled synthesis of inorganic phases at the micro- to nanometer scale crystal engineering of bulk solids and assembly of organized composite and ceramic materials is a future perspective of great importance. Nacre is therefore a promising model for new polymer/mineral composite material synthesis.

We want to report here on the structure, properties and growth of columnar (gastropod) nacre with emphasis on the genus *Haliotis* (abalone) in contrast to sheet nacre of many *bivalves*. Most frequently abalone nacre from the species *H. rufescens* (red abalone) and *H. laevigata* (greenlip abalone) is investigated. For these species, the dimensions of the individual mineral layers are similar, whereas other less frequently used species such as *H. iris* and *H. fulgens* are known to have somewhat thinner mineral layers [8]. For a review on sheet nacre please see a recent review from Meyers et al. [9].

2. Structure

The shell of most of the gastropod snails is divided into a calcitic and an aragonitic part [10]. Both of them are calcium carbonate polymorphs with the same chemical formula ($CaCO_3$) but different crystal structure.

2.1. Coarse structure of nacre

2.1.1. The mineral part

The shell is composed of more than 95 wt.% of mineral. When aragonite is present in a shell it is located in the inner part, facing the animal. The surface is very smooth and usually shows two different

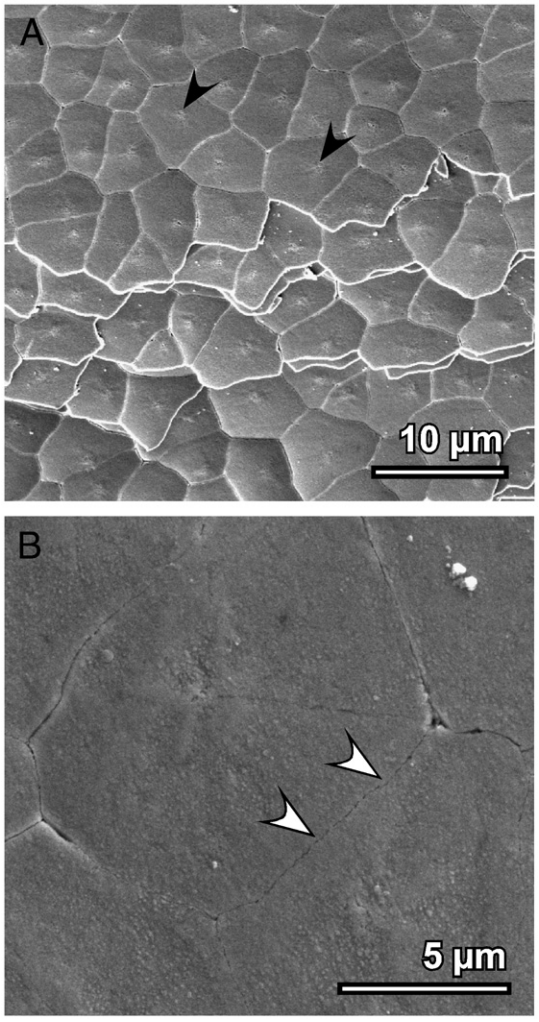

Fig. 2. SEM images of a longitudinal fracture surface of nacre of the shell of *Haliotis laevigata.* A. The mineral layers are constructed of confluent polygonal platelets with a diameter of 5 to 10 µm. In the middle of each platelet a distinct structure is visible (black arrows). Possibly the contact area with the next vertically connected platelet. B. Close-up view on one of the platelets showing their tight connection to each other (white arrows).

structures: the edge region or growth front, which looks whitish and not iridescent (for explanation see Section 3 of this review, Fig. 19) and the main part, which is very shiny and displays all rainbow colours.

Nacre is constructed of confluent tablets, with a diameter between 5 and 10 μm (see also sketch in Fig. 3) forming a hierarchical structure with two levels — the single platelets itself as the subunit and the material composed of these platelets [11].

Looking at a cross fracture surface of nacre in the tens of micrometer range several different structures appear. The main ones are the highly organised aragonitic layers formed during the growth period and interdispersed mesolayers, which were created at periods, when in certain intervals no growth takes place [12,13]. The mesolayers are aragonitic block-like structures (TEM data, not shown). At the growth front, where the shell expands, "stacks of coins" are visible composed of aragonite platelets, where new single crystals appear before the underlying ones are confluent [14–17] (see also Section 3).

In a longitudinal fracture surface (Fig. 2) several layers (Fig. 2A) of mature nacre are displayed. The polygonal aragonite platelets are in close contact to each other (Fig. 2B, white arrows). There is a distinct structure in the middle of each platelet (Fig. 2A, black arrows), which might be the remnants of a mineral bridge (contact area between vertically connected tablets) and/or a different composition of the mineral.

2.1.2. The organic part, coarse structure

It is a central tenet in biomineralisation, that the organic matrix governs nucleation and growth of the mineral phase [5,17–20]. Although the organic phase represents less than 5 wt.% of nacre, it seems to be responsible for many processes taking place during shell formation.

At a first glance in SEM and TEM images, we find, that a large portion of the organic matrix is associated in layers between the aragonitic tablets (Fig. 3). In Fig. 1A SEM data are shown, where the growing crystals of the "stacks of coins" are visible. The vertical consecutive layers are interspersed with organic layers (Fig. 3A, black arrows), which could be detected because the sample has been treated with glutaraldehyde (2.5%), a crosslinking agent for proteins, before imaging. The upper part of the shell faces the animal and the epithelial cells of the mantle tissue (see also 20A). Several layers of organic sheets are deposited first by the animal, which are then grown in by aragonite crystals (Fig. 3A, black arrows) [21] through pores of diameters ranging from 50 to 200 nm [13,22]. In TEM images (Fig. 3B) of embedded, glutaraldehyde treated, EDTA (ethylenediaminetetraacetic acid) demineralised thin sections the structure of the interlamellar sheets can be obtained (Fig. 3B, black arrows). Besides these interlamellar sheets thin vertical walls are visible in the demineralised and the mineralised sample (Fig. 3B and C, white arrows). Thus we find in the coarse structure two distinct features, the "multi- or interlamellar sheets" [17] and vertical thin walls also called "intertabular matrix" [23]. The interlamellar sheets (or matrix), each constructed of several layers (and therefore also often called "multilamellar sheet"), are located along the mineral layers (usually horizontally). In sheet nacre Rousseau et al. showed AFM images of a foam like structure, which is attributed to intracrystalline proteins [24]. In columnar nacre it is also assumed that protein molecules are embedded into the mineral tablets. These proteins form the third organic feature — the intracrystalline proteins. A sketch of the coarse structure of nacre is shown in Fig. 3D.

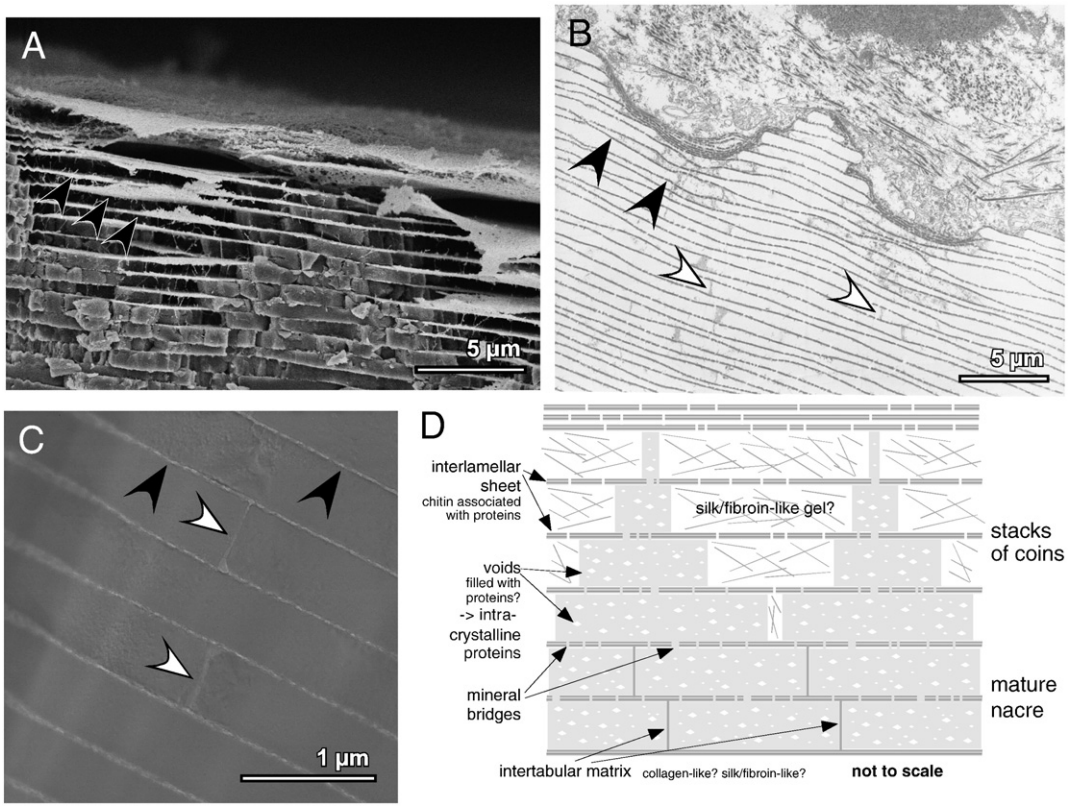

Fig. 3. Coarse structure of the water-insoluble organic layer of the shell of *Haliotis* tuberculata (A and B) and *laevigata* (C). A. SEM image of a glutaraldehyde treated and critical point dried section of the growth front. Organic layers (black arrows) are visible between each of the mineral platelets spanning also the distance between the platelets in the "stack of coins". B. TEM image of an embedded section of the demineralised growth front. The horizontal organic layers are connected by vertical organic structures (white arrows), the intertabular matrix (see also Section 2.3). C. TEM image of a thin section of mature nacre. The organic matrix surrounds each tablet (black and white arrows). D. Sketch of the growth front of nacre. Shown are the "stacks of coins" and confluent mature nacre. The interlamellar sheets (matrix) are secreted first and their interspaces get probably filled then by a gel of silk/fibroin-like proteins. Aragonite platelets grow between the interlamellar matrix until they are confluent. The platelets contain voids (probably filled by intracrystalline proteins) and are connected by mineral bridges. Laterally between the platelets there is an intertabular matrix, which might consist of collagen and/or silk/fibroin-like proteins.

Thus we find three protein groups, which we can classify by the coarse structure of the organic part.

A classification due to preparational issues is given in Section 2.3.

2.2. Fine structure of mineral platelets

2.2.1. The single platelet in nacre

It is generally accepted that the single, polygonal shaped platelets are crystals with roughly horizontal *a* and *b* axes (parallel to the interlamellar matrix) and roughly vertical *c* axis (perpendicular to the interlamellar matrix). The aragonite unit cell is orthorhombic with an *a* and *b* axis spacing of 4.95 and 7.96 Å and a *c* axis spacing of 5.74 Å.

The orientation of the crystallographic parameters have been studied by several groups. Whereas the morphology in geologically grown aragonite is needle like, with the fast growing axis being the *c* axis, gastropod nacre crystals are tabular ("tablets" and "platelets") [14,25]. Tablets for new mineral layers grow in small stencils or needles in the fast growth direction *c* (along the (001) direction) until they reach a height of about 500 nm, then they broaden in *a* and *b* direction until they become confluent [1,2] by reaching the lateral next tablet at a diameter of 5 to 10 μm (see also Section 3).

The question, why nature constructs nacre from subunits in the micrometer range, might be answered by considerations of Gao et al., who modelled the fracture strength of mineral platelets with incorporated proteins (flaws). Their model implies, that material constructed from nanometer subunits might be less sensitive to flaws [34] (see Section 2).

There is an ongoing discussion if one tablet (or even several tablets in vertical direction) is (are) a single crystal. In 1935 Swamy [27], reported about X-ray diffraction measurements on gastropods and the genus *Haliotis*. He stated that the platelets in three different *Haliotis* sp. are single crystals with slightly different (but somewhat preferred) *a* and *b* axes orientation along the columns. Which kind of *Haliotis* sp. he used for the measurements is not stated. In some other work [28,29] it is shown, that each tablet is divided in sectors by organic membranes in the vertical direction. The 2 to 50 sectors can be made visible by slight demineralisation of the tablets.

Investigating shell microstructure and crystallographic textures (distribution of crystallographic orientations of a polycrystalline sample) and their interplay in different shells of different mollusc groups in SEM and X-ray analysis, Chateigner et al. [30] conclude that there is no clear relationship between shell microstructures and crystallographic orientation. Crystallographic properties do not determine the morphology of the shell and the structure of the shell does not determine the crystallographic orientation. Thus both features are thought to be independent. Other authors find, that the aragonite tablets are single crystals with one or multiple twins [2,16].

To answer the question whether aragonite tablets in nacre are single crystals or built-up by many oriented nanocrystals and/or several larger sections, detailed TEM studies would be necessary.

One would expect from the surface of an ideal crystal being smooth and flat; the surface of aragonite platelets in nacre is pretty rough and corrugated (see Fig. 1C). It possesses nanoasperities, with some of them even protrude the interlamellar matrix as mineral bridges (Fig. 4) [31,32]. The nanoasperities show a diameter of 30 to 100 nm

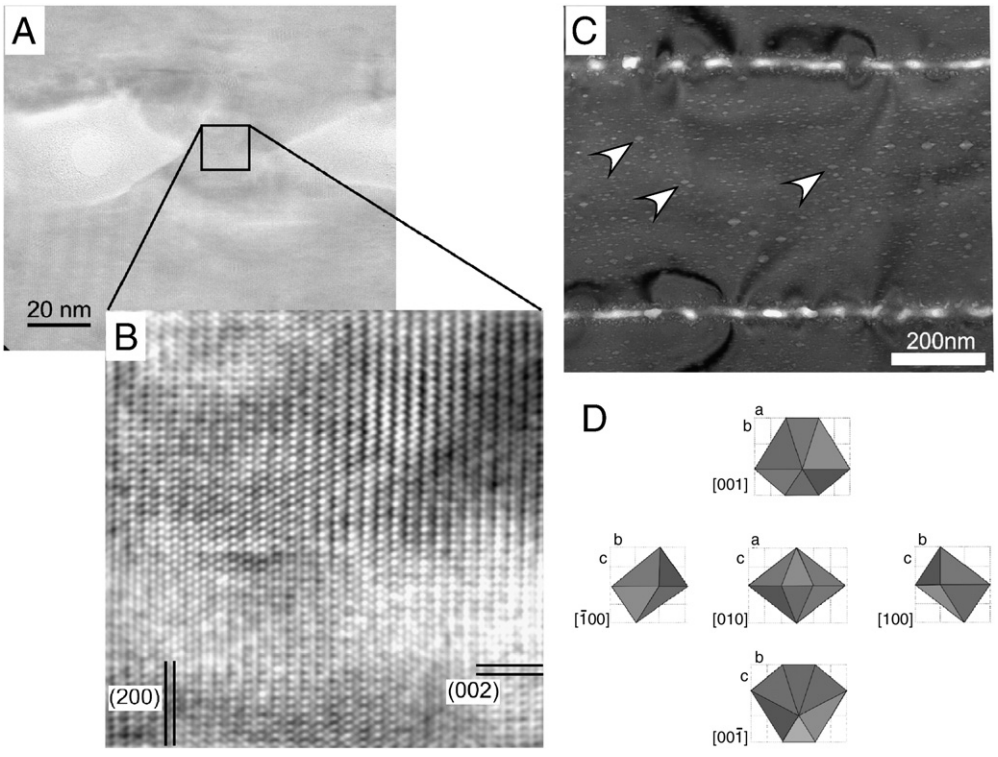

Fig. 4. Cross section of a thin lamella imaged in HR-TEM (high resolution transmission electron microscopy). A. TEM image of a mineral bridge, oriented in zone axis (010). A piece of nacre was cut with a diamond saw, thinned first mechanically and afterwards with a gallium ion beam in the FIB (focused ion beam) to a thickness of about 50 nm. B. Lattice planes of the crystalline material aragonite. It is obvious that the crystals protrude through the interlamellar matrix without changing the orientation supporting the idea that the platelets are connected by mineral bridges. C. TEM image of a thin lamella (cross section) of a platelet. The faceted voids (arrows) are clearly visible. D. Model of a void drawn from different perspectives. The lattice constants and the crystallographic orientation are specified.
Reprinted from Gries, K., Kröger, R., Kübel, C., Schowalter, M., Fritz, M., and Rosenauer, A. (2009) Correlation of the orientation of stacked aragonite platelets in nacre and their connection via mineral bridges, Ultramicroscopy 109, 230–236, with permission from Elsevier [32] and Gries, K., Kröger, R., Kübel, C., Fritz, M., and Rosenauer, A. (2009) Investigations of voids in the aragonite platelets of nacre, Acta biomaterialia 5, 3038–3044, with permission of Elsevier [35].

and a height of about 10 nm. The diameter of the mineral bridges in the range of 30 nm and the density of both features together (nanoasperities and mineral bridges) has been measured to be about 90 to 120 μm^{-2} [21,33]. Apart from these small corrugations of the platelet surface there is a waviness in terms of a larger wavelength undulation of the surface on the several micrometer range [112]. Nanoasperities and waviness are thought to have an influence on the mechanical properties (see Section 2).

For the growth of nacre in gastropods (and bivalves) there are several hypotheses (see Section 3). One of them include the mineral bridges growing through pores in the organic matrix being responsible for the nucleation of the next vertical tablet growth in *c*-direction maintaining the crystallographic alignment. The existence of the mineral bridges has been proven by visualising lattice planes of the crystalline material aragonite in HR-TEM (high resolution transmission electron microscopy). It is obvious that the crystals protrude through the interlamellar matrix without changing the orientation, because the lattice planes can be detected over the whole distance from the lower to the upper platelet (Fig. 4B).

Another puzzling feature of the platelets is that they obviously are not through and through solid, like one would expect from a crystal (single and/or polycrystalline), but that there are faceted intracrystalline voids several nanometers in diameter (Fig. 4C and D) [35]. The calculated volume in a platelet is about 0.2%. EDX (energy dispersive X-ray spectroscopy) and EELS (electron energy loss spectroscopy) measurements indicate a higher concentration of carbon in the voids in comparison to the bulk material, which could be a hint for organic material in the voids (intracrystalline proteins for instance).

2.2.2. Ordering of nacre tablets in and between columns

The nacre platelets are horizontally aligned in layers and vertically in columns. The orientation of platelets in the layers and columns has been investigated by HR-TEM, synchrotron spectroscopy and X-PEEM (X-ray photoelectron emission spectromicroscopy). To know the precise orientation of the crystals in the layers and columns could eventually help to unveil the secret of nacre growth. Important information is given by Metzler et al. and Gilbert et al. in [36–38]. They find, that the aragonite tablets in the first layer do have their *c* axis not perfectly aligned to each other with a gradually developing order with the distance of 50 µm from the boundary between calcite and aragonite in *Haliotis* (Fig. 5). They conclude that this is due to crystal

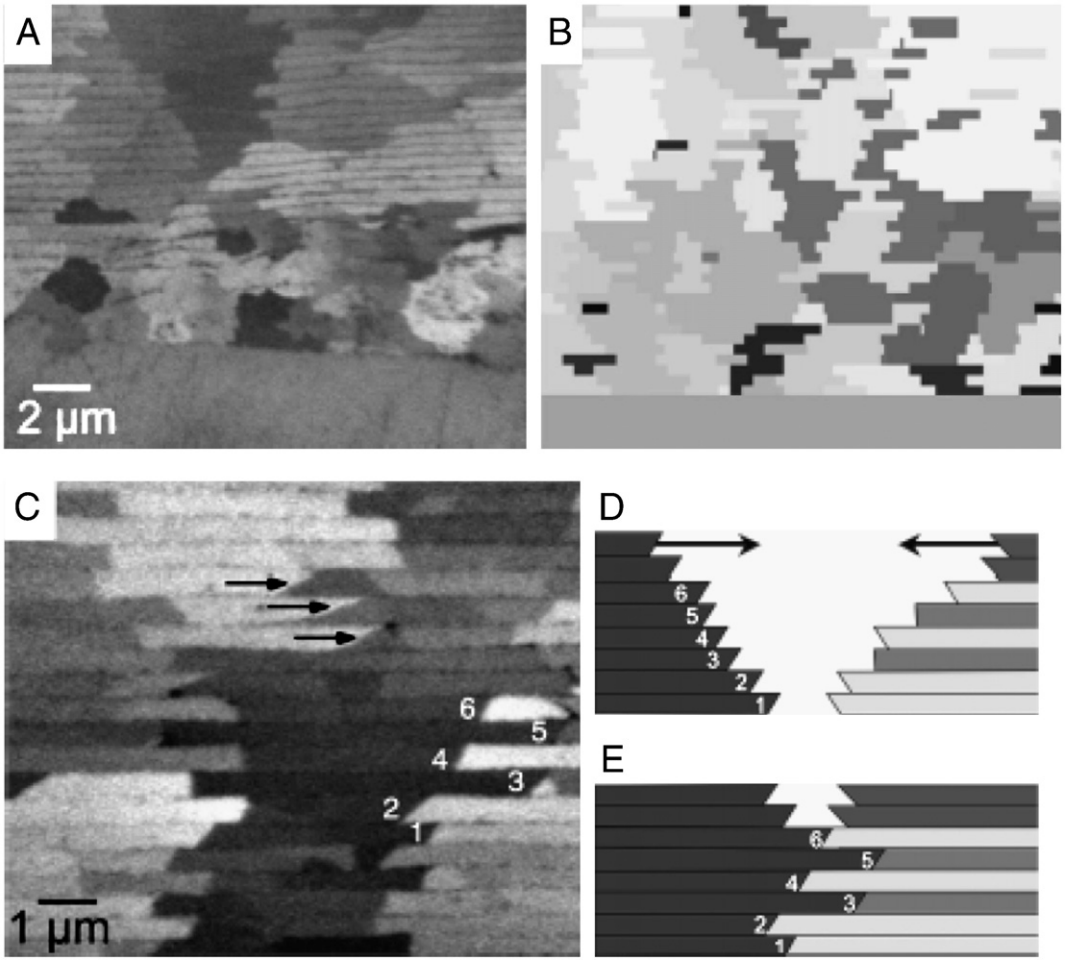

Fig. 5. Images of the orientation of nacre tablets in *Haliotis rufescens*. A. Experimental PIC (polarisation-dependant imaging contrast) data on nacre ordering at the nacre (top) to prismatic calcite (bottom) boundary. Tablets with the same grey level do have the same crystal orientation. The ordering in *c*-direction is increasing from the boundary to the volume fraction. B. Data from simulations, where each layer of tablets is given to complete before the tablets of the next one are nucleated. The different grey levels indicate different growth rates. The ordering in *c*-direction is gradually increasing. C. High resolution carbon PIC map of *H. rufescens* nacre near the boundary between nacre and prismatic calcite. Co-oriented tablets in the same stack show similar angles (black arrows) in horizontal tablet–tablet contact. This can also be seen in the boundaries between the tablets 1 to 6 and the horizontally adjacent ones. D. Schematic representation of a stack of tablets (1 to 6) during growth. E. Schematic representation of the stack in B at a later time assuming the grey levels being the slow growing tablets maintain their facets, whereas the fast growing ones fill the whole space.
These data are a valuable contribution of P. U. P. A Gilbert, Department of Physics, University of Wisconsin, reproduced with the kind permission of the publisher (copyright 2008 American Chemical Society). Reprinted with permission from Gilbert, P., Metzler, R., Zhou, D., Scholl, A., Doran, A., Young, A., Kunz, M., Tamura, N., and Coppersmith, S. (2008) Gradual ordering in red abalone nacre, J. Am. Chem. Soc 130, 17519–17527 [37].

growth kinetics rather than templation by organic material and therefore mineral phase is responsible for the growth properties.

Gries et al. have shown that in the range of a few tablets from the middle of the shell (18 tablets were investigated [32]) the tilt angle is less than 10° (*c* axis), thus the orientation is strongly correlated over this distance. Together with the observation of mineral bridges it is concluded that the growth process depends on small nucleation sites of the mineral (mineral bridges from the underlying layer) [32].

However, the *de novo* nucleation of the initial aragonite platelets cannot be explained by mineral bridges. Most likely, surface mediated nucleation and growth via mineral bridges are both required. We try to shed light on this in Section 3.

2.3. Organic material: molecular components and interactions

Molecular structuring is achieved by a high level of physico-chemical and spatial control over the precipitation process most presumably by protein molecules. However, the molecular interactions governing the formation of highly defined nanostructures have remained hidden. Some hints are given by investigations of the organic components in nacre.

The total organic material may be classified into three major groups: the interlamellar matrix, the intertabular matrix and the intracrystalline/tablet associated matrix. In this case the location of the material is the basis of the classification.

There is another possibility to classify the organic material: by means of solubilisation from the composite nacre. Here the "affiliation" of the different molecules is not unambiguous. There is the division "water soluble" versus "water insoluble" but hardly anyone solubilises nacre in water, because due to the solubility product of calcium carbonate (6×10^{-9} mol^2/l^2) it would take forever. So one may divide the organics in acid soluble and acid insoluble, but then one has to account for the concentration of the acid used. Perlucin for instance belongs to the interlamellar matrix, when the mineral is dissolved in 6% acetic acid, and to the tablet associated matrix, when the mineral phase is removed by 50% acetic acid. This also holds for solubilising the mineral with EDTA (ethylenediaminetetraacetic acid). This would be then the EDTA soluble fraction, where the concentration is important as well, and the EDTA insoluble fraction. Although this is the most gentle method, the issue is here, that Ca^{2+} dependant proteins (like C-type lectins) often lose their Ca^{2+} (sometimes irreversible) and therefore some of their function.

In the following we try to precisely classify the proteins either by their location (when known) or their solubilisation method.

2.3.1. The interlamellar matrix and the intertabular matrix

The interlamellar matrix is a multilamellar sheet of different kinds of organic material: proteins and polysaccharides. Whereas the polysaccharide chitin (N-acetylglucosamine or 2-(acetylamino)-2-deoxy-D-glucose) is straight forward to identify and locate; the identification and location of the different protein species is more difficult.

Removing the mineral component by a diluted acid or EDTA a honey comb-like pattern of organic material appears [39], which has been imaged with different techniques like AFM [21] and SEM [22]. Detailed light microscopic investigations including immuno-mapping has been done for bivalves so far [23]. The honey comb-like pattern is formed by the interlamellar matrix and the polygonal intertabular matrix (Fig. 6). After demineralisation the surface has an appearance of tightly packed globular structures showing a distribution of diameters in the range of tens of nanometers. In the middle of each honey-comb a pore is visible (Fig. 6B, white arrow). This might be the canal, where the platelets are vertically mainly connected, apart from the many other smaller mineral bridges. The area of single honey combs seems to be covered by proteins, where close to the pore acidic proteins have been reported for bivalves [23]. The proteins can be removed from the core by proteinases (like proteinase K).

Chitin forms the core component of the interlamellar matrix [40–42]. (There have been earlier reports in French, in which the authors are not fluent enough to understand [43,44]). It is a thin layer of ten to 30 nm, where the chitin filaments are forming a network leaving pores in the sheet of a diameter of up to 100 nm, where ions and protein molecules can protrude (Fig. 6C) [21]. Chitin is a chemical and mechanical very stable polymer, which might be also responsible for the corrosion resistance of the whole composite. There have been investigations, which suggest, that silk/fibroin-like proteins are attached to the chitin core [45]. X-ray diffraction of insoluble matrix showed pattern, which are consistent with the β-pleated sheet of various fibroins [46], which would fit nicely to the ion pattern of the *a*/*b* plane of the aragonite crystals. Furthermore they state, that the amino acid content (more than 50% of glycine, alanine and serine) of the investigated proteins resemble those of silk/fibroin [47]. In *in vitro* experiments of β-chitin purified from the pen of the squid *Loligo* and silk from the cocoons of the silkworm *Bombyx mori* have shown that using these polymers together as a substrate for aragonitic protein macromolecules aragonite crystal growth may be induced [19].

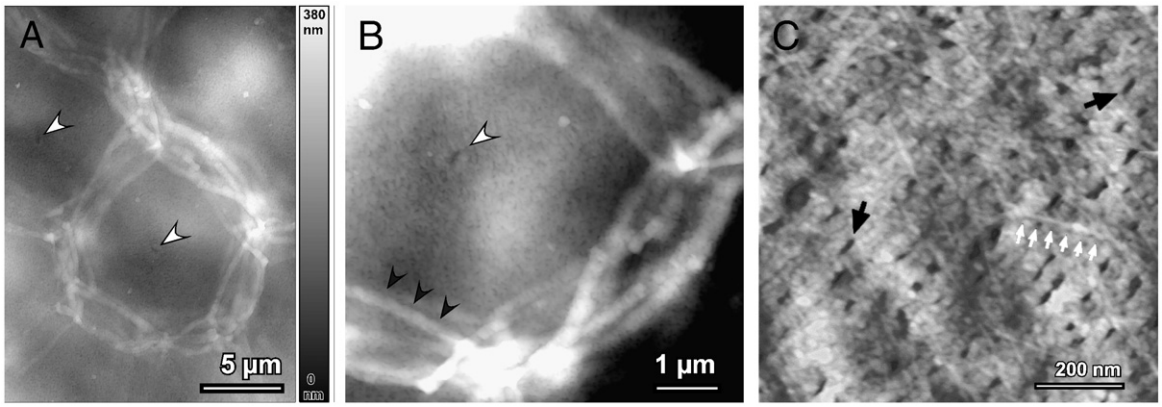

Fig. 6. AFM images of the longitudinal structure of the interlamellar sheet of the organic components of the shell of *Haliotis laevigata*. A. Surface of the demineralised organic (interlamellar) sheet. The imprint of the tablets shows a honey-comb like structure with a distinct structure in the middle (white arrows), where a mineral bridge could have been protruded. B. The close-up view of A. on one of the imprints shows tightly packed globular structures and a pore-like structure in the middle (white arrow). The intertabular matrix of several collapsed layers is visible (black arrows). C. Close-up view of B at the inner area of the imprint after proteinase K treatment. A filamentous chitin network with pores of about 50 nm (black arrows) becomes visible.

But until now (to the best knowledge of the authors) no silk/fibroin-like protein has been characterised yet in purified form from nacreous shells. In *Pinctada fucata* (bivalves) a protein (MSI60) was found by isolation of its cDNA, which contains poly(alanine) blocks similar to spider dragline silks [48]. In situ hybridisation [49] of the mantle epithelium shows that it expresses MSI60 mRNA (see also Section 3).

Bezares et al. mapped the macromolecular structure of the protein surface of the interlamellar matrix in *Haliotis rufescens* [22]. They found distinct regions concerning the distribution of different types of molecules by employing staining methods with WGA (wheat germ agglutinine) gold and polyclonal antibodies against aragonite nucleating proteins [50]. WGA gold stained preferably the intertabular matrix (which showed a kind of double-walled structure between the removed mineral tablets), indicating a high content of glycoproteins and chitin. But also the staining with the antibodies showed that aragonite nucleating proteins are distributed all over the matrix. Sulfates and carboxylates showed in this study to be mainly distributed at the ring area close to the intertabular matrix.

The intertabular matrix is an organic ring like structure located laterally between the aragonite tablets. After demineralisation it mirrors the outline of the tablets (see also Fig. 6A and B). As it can be degraded by proteases it seems to at least contain (probably besides chitin) proteins.

In TEM images of intact nacre the intertabular matrix is hard to recognise [13]; thus it seems to have a diameter of much less than 50 nm, which is the thickness of the well observable interlamellar sheet.

2.3.2. The intracrystalline matrix (diluted acetic acid and EDTA soluble proteins)

Actually there is no protein species reported, which has been purified from nacre platelets themselves (after removing the interlamellar and intertabular organic matrix) as a subspecies of the complete organic matrix of the shell of gastropods.

Thus this section will describe proteins of gastropod shells, which have been purified by demineralisation with 3 to 12% acetic acid and/or EDTA (up to 100 mM). But it might be, that these proteins are not only intracrystalline ones but also dissociated from the interlamellar and the intertabular matrix during preparation.

Thus the protein species reviewed in this section may belong to the interlamellar, intertabular and/or intracrystalline group.

Several proteins have been reported to be extractable from the shells of gastropods with means of dilute acidic acid and/or EDTA. Some of their functions are recently reviewed by Evans [51] and Marin and Luquet [52]. Evans details especially the terminal sequences of nacre and prismatic (calcitic) proteins and their possible function in protein/mineral interaction. Marin and Luquet report about 16 molluscan shell proteins, which primary sequence has been discovered so far (until 2004). Lustrin A, AP7, AP24, perlustrin and perlucin from gastropod columnar nacre are discussed concerning their biochemical features and the properties they share. They seem to be a heterogeneous group, which shows just little homologies or analogies to other proteins. Some amino acids like glycine, aspartic acid, serine, proline, cysteine, tyrosine, leucine and asparagine appear to be predominant. Some features like a modular construction in functional domains are discussed. One of them being the domain to interact with the mineral calcium carbonate. Some of them, like lustrin A carrying their own protease inhibitor.

Here we want to give an overview of those proteins, which are purified from columnar nacre of the genus *Haliotis* and their primary structure gained either by complete cDNA sequence or by protein sequencing.

The amino acid composition of nacre proteins has been investigated several tens of years ago [53]. Their measurements showed for the gastropod *Plicatula plicata* a high fraction (more than 25% of asx (aspartic acid + asparagine)) for the whole shell. It has been postulated, that proteins with high percentage of acidic residues might serve in the interlamellar matrix (acid or EDTA soluble part) as nucleation spots for aragonite crystallisation. A few years later Nakahara took the inner (nacreous) layer of *Haliotis rufescens* and an amino acid analysis revealed similar content of asx [5]. Some other groups also reported high fractions of asx and gsx (glutamic acid + glutamine) for *Haliotis* nacre [47,54].

In our group the amino acid composition of *Haliotis laevigata* nacre was highly dependant on the purification method [55]. Heinemann reports after amino acid analysis that the most prominent residues detected, were proline, glycin and leucin (Table 1). This fits well to the primary sequences of perlucin, perlustrin and perlwapin [56–58] (Table 2).

Just for the protein mixture, which has been purified by C18 ZipTips (pipette tips filled with hydrophobic material), aspartic acid was with about 14% the most prominent residue.

The reason for this difference is unclear. As our study was the first, which has been performed for nacre proteins of *Haliotis laevigata* it might be that there are some additional/different proteins in this shell species, which change the overall amino acid composition. For instance perlucin is the most prominent protein in nacre of this species. Especially for this protein the purification method is essential. The higher the acidic acid concentration (higher than about 6%) during demineralisation of nacre the more perlucin solubilises. With more gentle demineralisation perlucin stays at the interlamellar matrix probably as chitin binding protein.

In Fig. 7 two representative SDS PAGEs are shown (provided by Meike Gummich, Pure and Applied Biomineralisation Group, Biophysics Institute, University Bremen, Germany). Fig. 7A shows proteins, which are not or weakly soluble during demineralisation of columnar nacre in up to 6% acetic acid. They are potential interlamellar matrix proteins connected to the core of chitin or some linker protein. In Fig. 7B soluble (following these conditions) proteins are displayed on the gel. Perlucin (band beneath the 21 kDa marker, white arrow) is visible on both gels. This might also hold for AP8 (grey arrow), which is presumably the band above the 6 kDa marker.

With varying demineralisation conditions the ratio of the concentrations between the “insoluble” and the “soluble” fraction changes.

Perlucin [56] is the highest concentrated protein in nacre of *Haliotis laevigata*. Perlucin is a C-type lectin; a Ca^{2+} dependent

Table 1
Amino acid compositions of soluble matrix fractions after different purification procedures. The values represent average molar fractions in %. The three most abundant amino acids are printed in bold numbers. Cya corresponds to the cysteine content. Asx stands for Asp + Asn, Glx for Glu + Gln.

Amino acid	Ultra-centrifuge purified	Cation exchanger purified	C18 — ZipTip purified
Asx	1.0	4.6	**14.1**
Glx	2.9	5.7	6.5
Ser	3.7	6.2	5.9
Gly	**11.7**	**8.6**	**13.3**
His	2.0	2.0	6.9
Arg	1.0	3.1	2.5
Thr	6.1	6.9	3.7
Ala	8.1	8.0	8.5
Pro	**24.7**	**13.8**	**9.4**
Tyr	3.5	3.8	3.1
Val	4.2	5.7	4.4
Met	3.4	7.6	1.0
Ile	2.7	4.2	3.7
Leu	**8.3**	**8.5**	7.1
Phe	4.8	4.6	4.3
Trp	5.6	1.5	0.5
Lys	5.3	3.2	3.7
Cya	0.8	2.2	1.4

Table 2
Proteins with primary sequence published from the organic matrix of the nacreous layer of the gastropod abalone (genus *Haliotis*). The isoelectric point (pI) was calculated using the ExPASy server (Swiss Institute of Bioinformatics) [185]. The first 5 proteins have been isolated from the nacrous layer of *H. laevigata*, the others from *H. rufescens*. Lustrin A is presumably an interlamellar matrix protein.

Protein accession number	Sequence accession number	MW [kDa]	Most dominant amino acids	Calculated pI	Possible function	Reference(s)
Perlucin	P82596 (UniProt)	18.155	Leu (9.7%) Arg (8.4%) Ser, Gly, Asn (7.7%)	7.2	Sugar binding, Crystallization enhancer	[39,56]
Perlustrin	P82595 (UniProt)	9.338	Cys (14.3%) Pro (9.5%) Leu (8.3%)	8.0	Insulin-like growth factor binding	[57,176]
Perlwapin	P84811 (UniProt)	14.528	Cys (18.7%) Pro (15.7%) Gly (11.9%)	8.6	Calcite growth inhibition	[58]
Perlinhibin	P85035 (UniProt)	4.793	Cys (19.5%) His (17.1%) Arg (14.6%)	8.3	Calcite growth inhibition, aragonite nucleation	[56]
Lustrin	AF023459 (GenBank)	142.209	Ser (16.4%) Pro (13.9%) Gly (13.4%)	8.1	Matrix-platelet adhesive, protease inhibitor	[60]
AP7	AF225916 (GenBank)	9.935	Leu (9.1%) Arg, Cys, Ser, Tyr (8.0%) Ala, Asp, Gly, Ile, Thr (6.8%)	5.5	Calcite growth inhibition	[62,177]
AP8 α, β	Not sequenced	7.8, 8.7	Gly (~39%) Asx (~35%) Glx (~8%)	–	Crystallization enhancer	[54,177]
AP24	AF225915	19.595	Thr, Asn (8.2%) Ala (7.0%) Asp, Val (6.4%)	5.8	Calcite growth inhibition	[62,177]

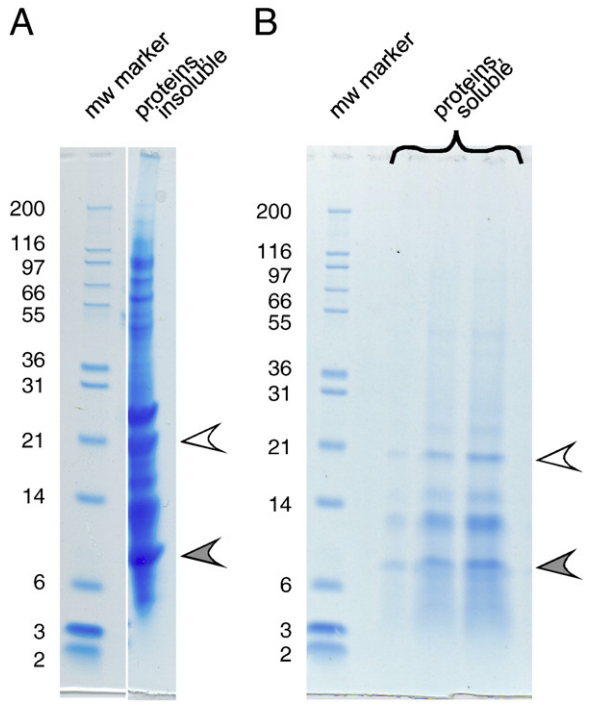

Fig. 7. SDS PAGE (sodium dodecylsulfate polyacrylamide gel electrophoresis) of acid (6%) insoluble and acid (6%) soluble proteins of the shell of *Haliotis laevigata* (provided by Meike Gummich, Biophysics Institute, University Bremen). A. Two lanes with protein bands are visible. The left one is loaded with protein markers of size indicated in kDa. The right lane shows protein bands extracted from the organic matrix, which has been treated with 6% acetic acid. These proteins were bound to the interlamellar matrix until treated with extraction buffer (20 mM Tris–HCl, pH 7, 10% Glycerol, 2% SDS). Note bands at molecular weight of about 8 kDa (grey arrow) and lane at molecular weight of about 18 kDa (white arrow). B. Four lanes with protein bands are shown. The left one is loaded with protein markers of size indicated in kDa. Next three lanes are different concentrations of 6% acetic acid soluble proteins. Note bands at molecular weight of about 8 kDa (grey arrow) and lane at molecular weight of about 18 kDa (white arrow). They appear in the 6% acetic acid insoluble and in the soluble fraction and are probably AP8 and perlucin respectively.

carbohydrate binding protein, which might also be connected to the chitin core. It has been shown to nucleate calcium carbonate crystals and to increase their growth velocity [39].

Perlustrin [57] is one of the higher concentrated proteins. From interaction studies with saturated calcium carbonate solutions it has not shown any influence on crystal growth. It has a certain relation to IGF (insulin growth factor) binding proteins and shown in *in vitro* studies to bind to IGF. It might interact with the mantle epithelial cells and be a part of their proliferation control.

Perlwapin [58] consists of 134 amino acids and contains three sequence repeats of about 40 amino acids which are very similar to the whey acidic protein (WAP) domains of other proteins. Direct AFM investigations during growth of calcium carbonate crystals show a strong growth inhibiting effect. Perlwapin molecules bind tightly to distinct step edges of calcium carbonate crystals preventing the crystal from growing.

Perlinhibin [59] is a crystal growth inhibitor as well. It is a very small protein (4.8 kDa) with an isoelectric point of 7.8. The sequence of 41 amino acids was determined by Edman degradation and by mass spectrometry. The most dominant amino acids were cysteine (19.5%), histidine (17%), and arginine (14.6%). It is a very compact protein with four active disulfide bonds. AFM studies revealed that the protein bound specifically to calcite steps, inhibiting further crystal growth at these sites.

The largest protein, which has been cloned and characterised by cDNA analysis is lustrin A [60]. The calculated mass of the protein is 116 kDa, but the native polypeptide chain extracted from columnar nacre of *Haliotis rufescens* has a MW of 65 kDa. The most striking feature is its modular design in the primary sequence: a cystein-rich and a proline-rich domain, which is repeated eight times each. It is thought to be a linker protein between the mineral and proteins and/or chitin in the interlamellear sheet [61]. It will be discussed in more detail in Section 2.4.

Two further aragonitic proteins from columnar nacre (*Haliotis rufescens*), AP7 and AP24 (aragonitic protein of MW 7 kDa and 24 kDa) have been deduced from mantle cDNA library [62]. Purification fractions with high AP7 and AP24 showed influence on calcium carbonate crystal growth. The first 30 N-terminal residues slowed down the growth of crystals. In circular dichroism (CD)

measurements these peptides show no secondary conformational structures like α-helices and β-sheets.

The two AP8 (aragonitic protein of MW 8 kDa) [54] proteins (AP8α and AP8β) have compositions dominated by asx (35 mol%) and gly (40 mol%) residues. In growth experiments (ammonium carbonate method [19]) AP8 proteins preferentially interact with defined step edges of calcite and accelerate the growth of acute edges, whereas the obtuse edges remained unmodified. This is one of the sparse experimental supports of the theory that preferentially acidic proteins interact with calcium carbonate crystals [63].

The raw extract of 6% acetic acid and/or 10% EDTA demineralised columnar nacre containing most of the previously mentioned proteins showed strong influence in precipitation of super saturated calcium carbonate solution [64]. At very low protein concentrations (0.02 μg/ml) a rate enhancement of factor 1.4 in comparison to the pure supersaturated calcium carbonate solution was observed. At higher protein concentrations, a strong inhibitory effect occurred, with total inhibition at concentrations of 1.0 μg/ml and higher. During shell growth the function of these proteins might be to prevent uncontrolled crystallization in the extrapallial fluid.

An overview of columnar nacre proteins with primary sequence and some other characteristics is shown in Table 2.

2.4. Organic–inorganic interface at the mineral platelets

One very important requirement for the outstanding mechanical properties of nacre is the strong contact between the mineral platelets and the organic matrix (see also the reviews [9–11,65–67]).

A recent review on organic/mineral interfaces in biomaterials is given by Gilbert et al. [68].

There is just a small number of experimental data about the molecular interactions between the organic and inorganic phase in gastropod columnar nacre available.

In the eighties Weiner et al. [40] performed electron diffraction on gastropod nacre samples, where the insoluble matrix (partially decalcified by 10% EDTA) was thought to be still intact and still in place on the aragonite tablets like in the natural material. They measured an area corresponding to the size of a single platelet and found in a few samples that the diffraction pattern of the aragonite crystal is well oriented with the polypeptide chain of the insoluble (10% EDTA) matrix. The polypeptide chain is oriented to the *b*-crystallographic axis and the chitin fibrils parallel to the *a*-axis. This would support a templating mechanism of the mineral crystals on the foremost secreted organic material (for further readings on growth hypothesis see Section 3).

Molecules in the interlamellar matrix of nacre have been tested by force spectroscopy [61]. The AFM tip has been brought to contact with the organic surface (in its native stage and still adhered to the mineral phase) and force-extension curves have been performed. Rupture events are visible with a sawtooth appearance. The authors explain their data by unfolding substructures on the molecular level (probably the modular constructed protein lustrin A) which form a adhesive constructed of several modules between the nacre tablets, which would lead to a higher energy required to break the material in comparison to a small molecule or a long molecule breaking late, but the force at low extensions would be small.

The organic/mineral interface has been probed on the molecular level by XANES (X-ray absorption near edge spectromicroscopy) in model biominerals. Metzler et al. [69] investigated calcium carbonate crystals grown (ammonium carbonate method [19]) in the presence of gastropod nacre polypeptides (AP7N, 30 amino acid N-terminal fragment and AP24N, 30 amino acid N-terminal fragment).

Spectra of pure calcite, pure polypeptides and calcite grown in the presence of each polypeptide have been taken. They showed that specific atomic bonds in calcite and specific bonds in the polypeptides change in the crystals grown with AP7N or AP24N. Both peptides induce a decrease in the C–O bond signal of the carbonate and an enhancement of the C–H and C–O bonds signal in the particular peptide. These measurements indicate an ordering of the polypeptide chains concurrent with the disruption of certain bonds in the calcitic part [69].

3. Physical and chemical properties

3.1. Optical properties of nacre

Handling shells the most obvious effect noticed are the colourful patterns on the nacre surface (Fig. 1A). In 1917 Pfund performed a study [70] investigating the reason of the iridescence of nacre from a mussel. The author could identify multilayer interference of light reflecting from the organic–mineral interface (Fig. 1B) as source of the colourful appearance of nacre (for a review of the physics of structural colours see [71]). From the aforementioned study a layer thickness between 400 and 600 nm was derived. Since the outer layer of shells is often composed of prismatic calcite optical phenomena are first visible upon removal of this layer. After careful removal of the calcitic part Pfund noticed a regular pattern of terminating layers from the nacreous area. The regularity and length scale of this surface leads to optical properties comparable to that of a diffraction grating.

Other studies (e.g. [72,73]) report similar groove structures on polished shell surfaces of *Pinctada margaritifera* and *Haliotis glabra* (Fig. 8) respectively. These microstructures are responsible for iridescence caused by light diffraction. In summary diffraction and multilayer interference contribute to the iridescence of nacre.

It seems to be that structural colouring of the outer shell surface is rare compared to the inner nacreous shell surface (e.g. [74]). The question whether the iridescence is just a result of the structure of nacre or serves another purpose cannot be answered to date (for a review of the multiple functions of iridescence in organisms see [75]).

3.2. Thermodynamic properties of the mineral phase

There are strong indications that the seawater chemistry – with respect to the Mg^{2+}/Ca^{2+} ratio – during the evolution of mineral skeletons/shells in a clade influenced the selection of aragonite or calcite as shell mineral (Fig. 9) [76,77].

While investigating the mineralogy of ancient ooids (sedimentary particles coated with calcium carbonate) and cements Sandberg [78] found an oscillating trend in the mineralogy. In recurring periods of time the formation of aragonite was preferred with respect to calcite and vice versa.

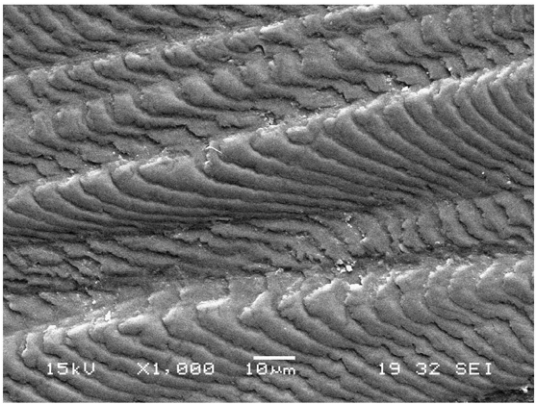

Fig. 8. Image of groove structures on a polished shell surface of *Haliotis glabra*. Reprinted with kind permission from [73].

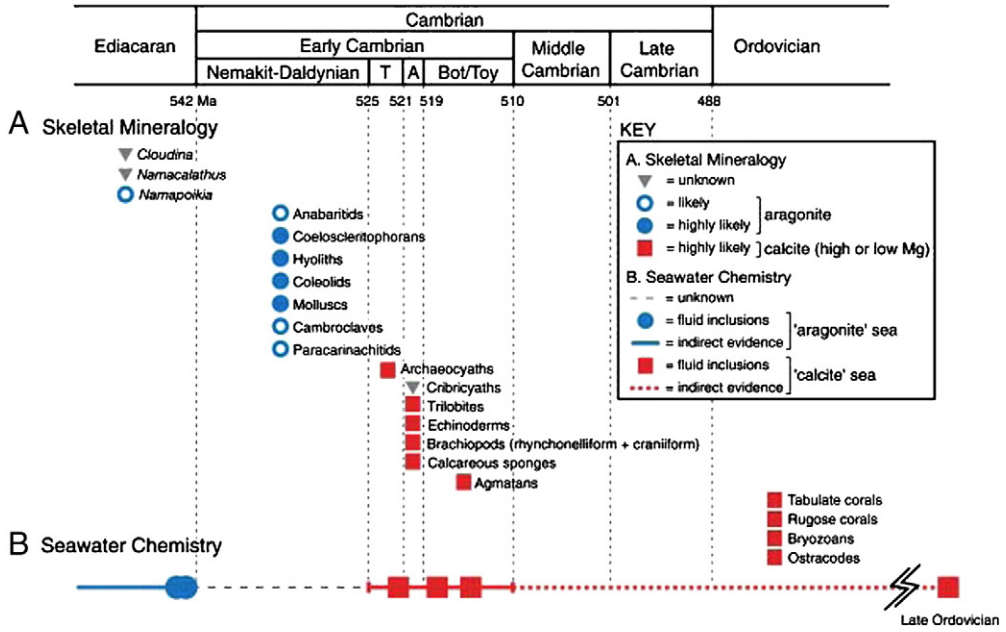

Fig. 9. A. First appearances of aragonite and calcite in skeletal mineralogy and B. the prevailing sea water chemistry. *Ma*: million years — *T:* Tommotian Stage — *A:* Atdabanian Stage — *Bot/Toy:* Botomian and Toyonian Stages.
From *S.M. Porter, Seawater Chemistry and Early Carbonate Biomineralization, Science, 316, p. 1302 (2007)* http://dx.doi.org/10.1126/science.1137284. Reprinted with permission from AAAS. The years given in this figure have been taken from the International Commission on Stratigraphy International Stratigraphic Chart (2007) and [184].

Lowenstein [79] and Hardie [80] found oscillations in the ion composition of seawater and especially in the Mg^{2+}/Ca^{2+} ratio. These variations correlate with the mineralogies of nonskeletal carbonates found by Sandberg in the sense that a ratio of approximately $Mg^{2+}/Ca^{2+}>2$ corresponds to aragonite and approximately $Mg^{2+}/Ca^{2+}<2$ favours calcite as mineral (information on the Mg^{2+}/Ca^{2+} threshold can be found in references given in [81] and [80]).

An influence of the magnesium to calcium ratio on the polymorph of growing calcium carbonate crystals is well known. Earlier studies of precipitation of calcium carbonate from artificial seawater (e.g. [82,83]) show that in present day seawater ($Mg^{2+}/Ca^{2+}\approx5$) the precipitation of aragonite and calcite with high magnesium content is favoured in comparison to calcite or calcite with low magnesium content. The authors of the last-mentioned study point out that the critical Mg^{2+}/Ca^{2+} ratio, where the precipitate changes from calcite to aragonite is temperature dependant. The critical ratio decreases with increasing temperature.

In the absence of magnesium in the system $CaCO_3$–CO_2–H_2O calcite has a lower equilibrium constant than aragonite under physiological conditions. It is log $K_{calcite}=-8.48$ and log $K_{aragonite}=-8.34$ at 25 °C [84]. Gutjahr and co-workers [85] showed that in this "pure" system the growth rate of calcite is larger than that of aragonite. Recently J.W. Morse and R.S. Arvidson reviewed the vast topic of dissolution kinetics of carbonate minerals [86].

Checa and co-workers [87] studied the response of bivalves with respect to shell mineralogy in magnesium enriched seawater ($Mg^{2+}/Ca^{2+}\approx8$ to 9). The chemical composition of the water forced the organisms – with predominantly calcitic shells – to produce aragonite on the inner shell surface instead of calcite. It has to be added that the best survival rate was around 63% for one species whereas other species died before the end of the experiment.

Furthermore the authors point out that some molluscs have both aragonite and calcite as shell constituents (for a taxonomic distribution of aragonite and calcite in bivalves see [88]). They conclude that if bivalves (as well as other molluscs) can form an outer calcite layer, even in seawater with high Mg^{2+}/Ca^{2+} ratio, this process must be biologically controlled (see Section 4 in this review). Checa et al. support this with the fact that the extrapallial fluid has nearly the same Mg^{2+}/Ca^{2+} ratio as seawater (see e.g. [89]).

The purpose of an outer calcite layer of mollusc shell (e.g. as protection against dissolution) in present day seawater seems to be unclear to date. See [90] for a general discussion and additionally Cubillas et al. [91] for dissolution rates of bivalve shells.

3.3. Mechanical properties of nacre

3.3.1. Introductory remarks

Recently Meyers and co-workers published an extensive review about the structure and mechanical properties of different biological materials [9]. Here we focus on the structure and mechanical properties of nacre of gastropods. Due to the massive amount of available literature dealing with this topic we cannot provide the citation of each available publication. This chapter should be regarded as a summary.

Wainwright commented already in 1969 [92] that shells of bivalves are remarkable composites of minerals and proteins. Shells are formed by the organism under ambient conditions and the formation process does not require non-physiological conditions often used during the production of artificial/man-made materials.

Nacre as a structural part of shells is composed of a mineral (approximately 95 wt.%) and an organic phase (Figs. 1 and 2). The single components of nacre, the mineral aragonite and the organic molecules (mainly proteins and chitin) exhibit "minor mechanical properties". Nevertheless if these constituents are arranged in a specific manner (Figs. 1B and 3) a composite with "superior mechanical properties" emerges. In the following the mechanical properties are summarised so that the aforementioned distinction between "minor" and "superior" is fortified by experimental results. Additionally the underlying mechanisms responsible for the outstanding mechanical properties are highlighted.

Efforts are being undertaken to understand design principles of nacre evolved during millions of years. It is being aimed to mimic the formation process of nacre and exploit the design principles with utilisation of the great variety of inorganic and organic compounds available to researchers (e.g. see [93–96]).

3.3.2. Mechanical properties of nacre in numbers

A quick but rough comparison of biological with some custom-engineered materials and other biological tissue is possible through material property charts [97,98].

Considering small isothermal deformations of an isotropic solid in the linear elastic regime the Young modulus E relates the stress σ to the strain ε of a solid according to

$$\varepsilon = \frac{1}{E}\sigma \tag{1a}$$

This is Hooke's law in a simple uniaxial tension notation. A more general formulation can be given in terms of a tensor formalism (see e.g. [99])

$$E_{ij} = \frac{1+\nu}{E}\sigma_{ij} - \frac{\nu}{E}\sigma_{kk}\delta_{ij} \tag{1b}$$

where δ_{ij} is the Kronecker Delta and ν describes the Poisson ratio. Rigorous mathematical derivations can be found e.g. in [100] whereas more descriptive representations are subject to undergraduate engineer textbooks (e.g. [101]).

Fig. 10 shows the specific Young modulus E/ρ (ρ denotes the density) plotted against the specific strength σ_f/ρ for various natural materials. Here σ_f is defined in a different way for each material class [97] but can in general be regarded as the applicable stress to a solid before permanent deformations or damage occurs. If the properties of the mollusc shell and aragonite and calcite respectively, which contribute the major part of the shell, are compared, a reduction of the specific modulus and an increase of the specific strength (at least of some shells) can be seen.

Nevertheless a look at Table 3 clarifies that the specific modulus and strength for mollusc shells – as a subset of natural ceramics and ceramic composites – is comparable to those of some steels and alloys.

Additional important quantities for the characterisation of a material are toughness or fracture toughness. These quantities describe the resistance of a material to propagation of cracks. For materials that obey Hooke's law following relations hold [102,103].

Considering a body containing a crack one can define an "energy release rate" G as the amount of energy available for an extension of the crack area A.

$$G = -\frac{d\prod}{dA} = -\frac{d}{dA}(W_{ela} - W_{ext}) \tag{2}$$

$\Pi = W_{ela} - W_{ext}$ can be regarded as the potential energy of an elastic body and therefore G is sometimes called "crack driving force". The potential energy of an elastic body is stated as the difference of the elastic energy W_{ela} stored in the solid and the work W_{ext} done by external forces. If G reaches a critical value $G = G_c = R$ a crack extension occurs. Consequently the critical energy release rate can serve as a measure of resistance of a material to cracks.

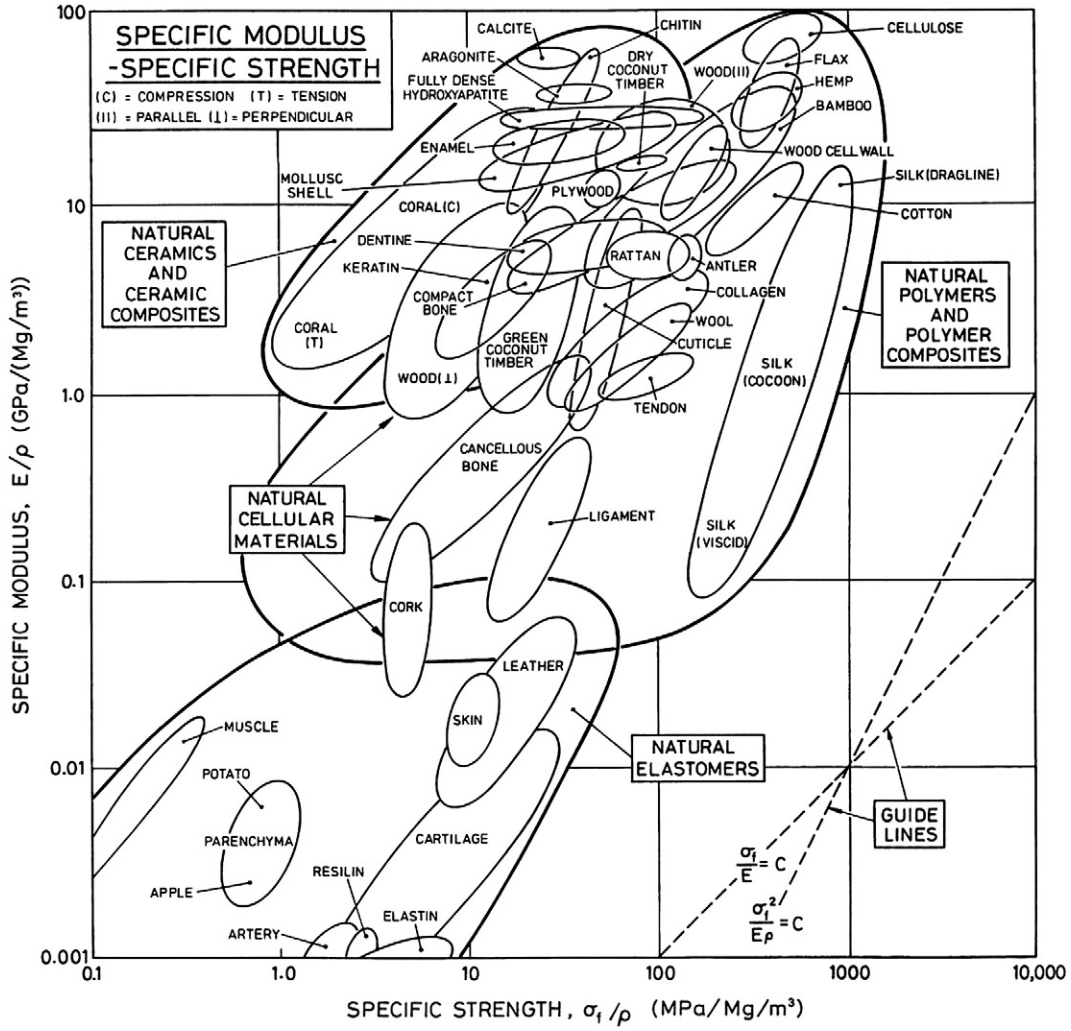

Fig. 10. Specific Young's modulus plotted against specific strength for various natural materials [98]. The data sources for the plotted values are given in the aforementioned reference. Reprinted with kind permission from Taylor & Francis Ltd. (http://www.informaworld.com/1478-6435).

Table 3
Specific Young´s modulus, specific strength and toughness of some common material classes. Approximate value ranges were taken from the materials selection charts given in [97].

Material class	Specific Young's modulus	Specific strength	Toughness
	GPa/(10^3 kg/m^3)	MPa/(10^3 kg/m^3)	kJ/m^2
Polymer foams	Up to 2	Up to 40	Up to 4
Elastomers (e.g. silicone rubber, polyurethanes)	Up to 0.2	Up to 50	
Engineering polymers (e.g. PTFE, PMMA, PP)	0.1 to 9	6 to 100	Up to 25
Engineering alloys (e.g. steels, aluminium alloys)	1 to 200	1 to 300	Up to 530
Engineering ceramics (e.g. alumina, zirconia)	15 to 300	300 to 7000	Up to 0.3
Porous ceramics (e.g. concrete, common rocks)	10 to 30	10 to 125	Up to 0.04
Engineering composites (e.g. fibre reinforced polymers)	10 to 100	100 to 1000	Up to 110

The resistance of material to crack extension R needs not to be a constant. R can depend on several variables, for example the crack extension. Toughening with crack extension ("rising R-curve") is caused by extrinsic toughening mechanisms (e.g. crack bridging). These mechanisms "act" behind the advancing crack opposed to intrinsic toughening mechanisms (e.g. crack-tip blunting in metallic materials) being independent of crack size and geometry (see [104]).

In this context one distinguishes the conditions of stable crack (crack length a) propagation

$$\frac{dG}{da} \leq \frac{dR}{da} \tag{3}$$

and unstable crack propagation

$$\frac{dG}{da} > \frac{dR}{da} \tag{4}$$

Another measure of crack resistance is provided by the stress intensity factor K. It describes the proportionality between the increase of local stress in the body and distance to the crack tip. The relation between K and the remote stress σ applied to a solid with a crack of characteristic dimension a

$$K = Y\sigma\sqrt{a} \tag{5}$$

Y is a dimensionless constant depending on the test geometry and mode of loading. The index "I" as it can be found in Fig. 11 refers to

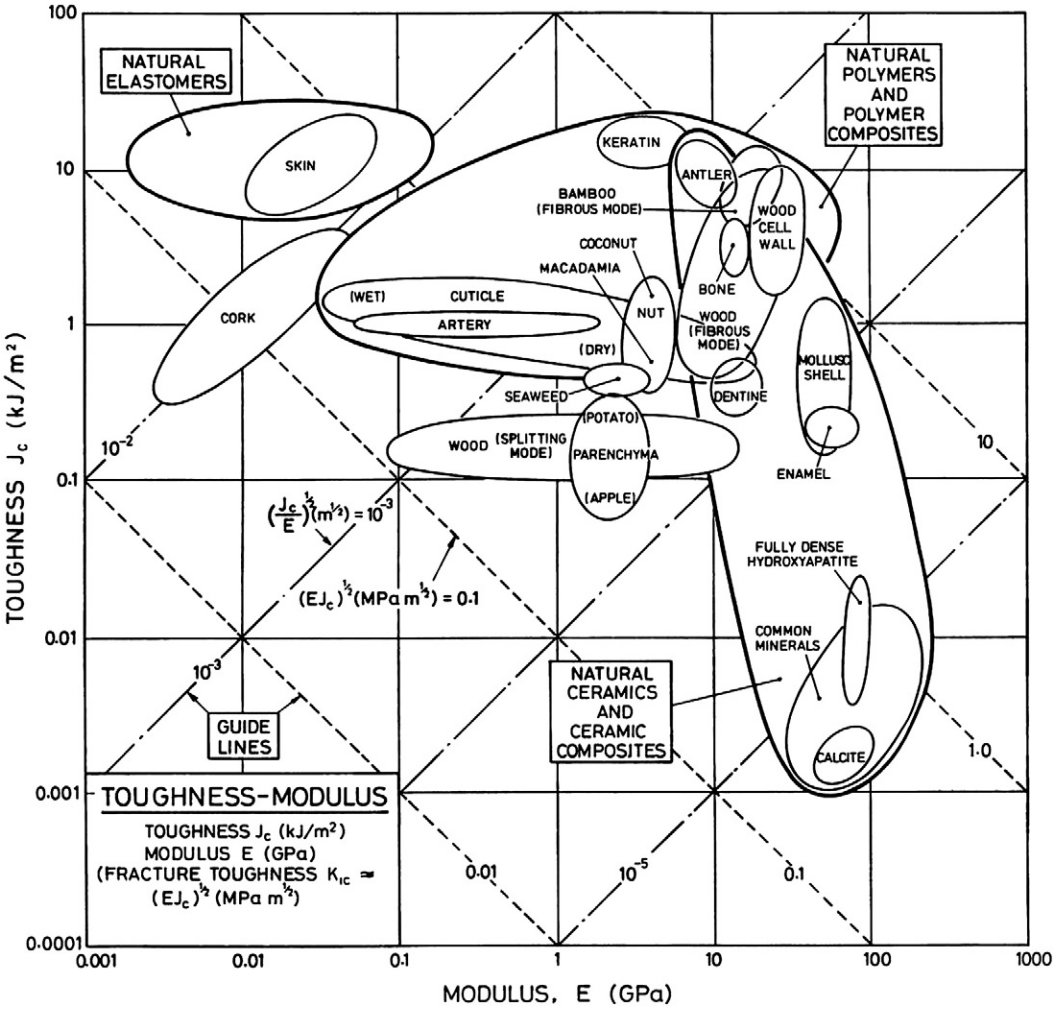

Fig. 11. Toughness plotted against Young's modulus for various natural materials [98]. The data sources for the plotted values are given in the aforementioned reference. Reprinted with kind permission from Taylor & Francis Ltd. (http://www.informaworld.com/1478-6435).

Table 4
Compilation of measured mechanical properties of mollusc nacre and shell respectively. The indicators of directions and planes are explained in Fig. 12. Bivalves are included in the section about toughness due to lacking measurements on gastropod nacre.

Value	Specimen (number of specimens)	Method	Comments	Animal	Author
Elastic modulus (values in GPa, round to integers)					
90	Nacre without the calcitic layer under dry conditions (2)	Quasi-static tensile test; tensile load ⊥ *z*-axis	Specimen shows linear elastic behaviour	*Haliotis rufescens*	[112]
80	Nacre without the calcitic layer under wet conditions (2)	Quasi-static tensile test; tensile load ⊥ *z*-axis	Determined in the initial linear regime	*Haliotis rufescens*	[112]
79 ± 15	Single dry aragonite tablet under ambient conditions	Nanoindentation; compressive load ∥ *z*-axis	Assumptions for properties of organic layers required	*Haliotis rufescens*	[125]
69 ± 7	Nacre without the calcitic layer under wet conditions (20)	Three-point bending; load ∥ *z*-axis	Flexural modulus	*Haliotis rufescens*	[33]
66 ± 2	Nacre without the calcitic layer under wet conditions (20)	Three-point bending; load ⊥ *z*-axis	Flexural modulus	*Haliotis rufescens*	[33]
70	Nacre without the calcitic layer under wet conditions (5)	Four-point bending; load ∥ *z*-axis; value for compression face	See [187] how to obtain compressive and tensile properties	*Haliotis rufescens*	[33]
8	Nacre without the calcitic layer under wet conditions (8)	Compression test; load 45° to *z*-axis	Cyclic loading reveals hysteresis indicating internal friction	*Haliotis rufescens*	[33]
114 ± 9	Freshly cleaved nacre tablet under ambient conditions (14)	Nanoindentation; compressive load ∥ *z*-axis	Depending on maximum loads; Oliver–Pharr-method	*Trochus niloticus*	[29]
103 ± 10	Hydrated nacre tablet under ambient conditions (14)	Nanoindentation; compressive load ∥ *z*-axis		*Trochus niloticus*	[29]
54	Shell pieces under wet conditions (4)	Three-point bending; load ∥ *z*-axis	Pre-dried samples were hydrated;	*Turbo marmoratus*	[105]
54 ± 6	Shell pieces under wet conditions (4)	Three-point bending; load ∥ *z*-axis	flexural modulus	*Turbo marmoratus*	[106]
64 ± 2	Shell pieces under wet conditions (3)	Three-point bending; load ∥ *z*-axis		*Trochus niloticus*	[106]
10	Nacre without the calcitic layer under wet conditions	Shear test; load ⊥ *z*-axis	Shear modulus; initial linear response	*Haliotis rufescens*	[112]
14	Nacre without the calcitic layer under dry conditions	Shear test; load ⊥ *z*-axis	Shear modulus; initial linear response	*Haliotis rufescens*	[112]
Strength (values in MPa, round to integers)					
135 and 95	Nacre without the calcitic layer under dry conditions (2)	Quasi-static tensile test; tensile load ⊥ *z*-axis	Ultimate strength	*Haliotis rufescens*	[112]
70	Nacre without the calcitic layer under wet conditions (2)	Quasi-static tensile test; tensile load ⊥ *z*-axis	Value when large deformation starts	*Haliotis rufescens*	[112]
250 ± 120	Single dry aragonite tablet under ambient conditions	Nanoindentation; compressive load ∥ *z*-axis	Assumptions for properties of organic layers required	*Haliotis rufescens*	[125]
223 ± 7	Nacre without the calcitic layer under wet conditions (20)	Three-point bending; load ∥ *z*-axis	Flexural strength	*Haliotis rufescens*	[33]
194 ± 8	Nacre without the calcitic layer under wet conditions (20)	Three-point bending; load ⊥ *z*-axis	Flexural strength	*Haliotis rufescens*	[33]
>370	Nacre without the calcitic layer under wet conditions (5)	Four-point bending; load ∥ *z*-axis; value for compression face	See [187] how to obtain compressive and tensile properties from	*Haliotis rufescens*	[33]
105	Nacre without the calcitic layer under wet conditions (5)	Four-point bending; load ∥ *z*-axis; value for tension face	four-point bending tests	*Haliotis rufescens*	[33]
160	Nacre without the calcitic layer under wet conditions (8)	Compression test; load 45° to *z*-axis	Cyclic loading reveals hysteresis indicating internal friction	*Haliotis rufescens*	[33]
540	Shell pieces under dry condition (7)	Quasi-static compression test, load ∥ *z*-axis	Weibull statistics [188] was applied; the given value indicates a 50% fracture	*Haliotis rufescens*	[128]
235	Shell pieces under dry condition (9)	Quasi-static compression test, load ⊥ *z*-axis	probability loading rates for dynamic tests in the order of $\approx 10^4$ *GPa/s*	*Haliotis rufescens*	[128]
735	Shell pieces under dry condition (13)	Dynamic compression test, load ∥ *z*-axis		*Haliotis rufescens*	[128]
548	Shell pieces under dry condition (14)	Dynamic compression test, load ⊥ *z*-axis		*Haliotis rufescens*	[128]
29 ± 7	Shell pieces under dry condition (6)	Shear test; load ⊥ *z*-axis	Ultimate shear strength	*Haliotis rufescens*	[128]
12	Shell pieces under dry condition (6)	Shear test; load ⊥ *z*-axis	Yield shear strength	*Haliotis rufescens*	[128]
20	Nacre without the calcitic layer under wet conditions	Shear test; load ⊥ *z*-axis	Yield shear strength	*Haliotis rufescens*	[112]
55	Nacre without the calcitic layer under dry conditions	Shear test; load ⊥ *z*-axis	Yield shear strength	*Haliotis rufescens*	[112]
108	Shell pieces under wet conditions (4)	Tensile test; tensile load ⊥ *z*-axis	Ultimate strength; pre-dried samples were hydrated	*Turbo marmoratus*	[105]
116 ± 15	Shell pieces under wet conditions (6)	Tensile test; tensile load ⊥ *z*-axis		*Turbo marmoratus*	[106]
85 ± 4	Shell pieces under wet conditions (4)	Tensile test; tensile load ⊥ *z*-axis		*Trochus niloticus*	[106]
353 ± 19	Shell pieces under wet conditions (10)	Compression test; load ⊥ *z*-axis	ultimate strength depends on aspect ratio; pre-dried samples were hydrated	*Turbo marmoratus*	[106]
320 ± 24	Shell pieces under wet conditions (5)	Compression test; load ⊥ *z*-axis		*Trochus niloticus*	[106]
267 ± 10	Shell pieces under wet conditions (4)	Three-point bending; load ∥ *z*-axis	ultimate bending strength; pre-dried samples were hydrated	*Turbo marmoratus*	[106]
220 ± 4	Shell pieces under wet conditions (3)	Three-point bending; load ∥ *z*-axis		*Trochus niloticus*	[106]
4	Fresh nacre without the calcitic layer (22)	Tensile test; tensile load ∥ *z*-axis	Weibull statistics (see [188]) was	*Haliotis rufescens*	[9]
210	Fresh nacre without the calcitic layer (12)	Compressive test; load ∥ *z*-axis	applied; the given value indicates a 50% fracture probability	*and Haliotis fulgens*	[9]
197	Processed shell pieces	Three-point bending; load ∥ *z*-axis	Flexural strength	*Haliotis rufescens*	[13]
177	Processed shell pieces	Three-point bending; load ⊥ *z*-axis	Flexural strength	*Haliotis rufescens*	[13]

(continued on next page)

Table 4 (*continued*)

Value	Specimen (number of specimens)	Method	Comments	Animal	Author
Strain					
0.01	Nacre without the calcitic layer under wet conditions	Quasi-static tensile test; tensile load ⊥ *z*-axis	Failure strain	*Haliotis rufescens*	[112]
0.001 and 0.01	Nacre without the calcitic layer under wet conditions	Four-point bending; load ∥ *z*-axis; value for compression face	Initial linear strain and failure strain (order of magnitude)	*Haliotis rufescens*	[33]
0.08	Nacre without the calcitic layer under wet conditions (8)	Compression test; load 45° to *z*-axis	Failure strain	*Haliotis rufescens*	[33]
0.45	Shell pieces under dry condition (6)	Shear test; load ⊥ *z*-axis	Maximum failure strain	*Haliotis rufescens*	[128]
0.15	Nacre without the calcitic layer under wet conditions	Shear test; load ⊥ *z*-axis	Failure strain	*Haliotis rufescens*	[112]
0.1	Nacre without the calcitic layer under dry conditions	Shear test; load ⊥ *z*-axis	Failure strain	*Haliotis rufescens*	[112]
Work of fracture/toughness/fracture toughness					
1.5 kJ/m^2	Nacre without the calcitic layer under wet conditions	Single-edge notched bending; notch in *yz*-plane; crack travels in *z*-dir.; load ∥ *z*-axis	Highest value; nacre toughens as crack grows	*Haliotis rufescens*	[112]
(1.65 ± 0.04) kJ/m^2	Shell pieces under wet conditions	Notched three-point bending; notch in *yz*-plane; crack travels in *z*-dir.; load ∥ *z*-axis	Work of fracture calculated from the area under the load-deformation curve; pre-dried samples were hydrated	*Pinctada margaritifera* (bivalve!)	[117]
(0.80 ± 0.08) kJ/m^2	Shell pieces under wet conditions	Notched three-point bending; notch in *yz*-plane; crack travels in *y*-dir.; load ⊥ *z*-axis		*Pinctada margaritifera* (bivalve!)	[117]
(0.15 ± 0.01) kJ/m^2	Shell pieces under wet conditions	Notched three-point bending; notch in *xy*-plane; crack travels in *x*-dir.; load ⊥ *z*-axis		*Pinctada margaritifera* (bivalve!)	[117]
(8 ± 3) MPa $\sqrt{m}$	Shell pieces	Notched three-point and four-point bending; crack travels in *z*-dir.; load ∥ *z*-axis	Stress intensity factor K_{IC} measured	*Haliotis rufescens*	[186]
(0.46 ± 0.14) kJ/m^2	Nacre without the calcitic layer under dry conditions (8)	Single edge notched three-point bending; notch in *yz*-plane; crack travels in *z*-dir.; load ∥ *z*-axis	Specimens loaded to failure; work of fracture calculated from the area under the force-displacement curve up to peak load; machine compliance corrected; span-to-depth ratio 4	genus: *Pinctada* (bivalve!)	[6]
(1.24 ± 0.78) kJ/m^2	Nacre without the calcitic layer under wet conditions (9)	Single edge notched three-point bending; notch in *yz*-plane; crack travels in *z*-dir.; load ∥ *z*-axis		Genus: *Pinctada* (bivalve!)	[6]
(0.44 ± 0.14) kJ/m^2	Nacre without the calcitic layer under dry conditions (9)	Single edge notched three-point bending, notch in *yz*-plane; crack travels in *y*-dir.; load ⊥ *z*-axis		genus: *Pinctada* (bivalve!)	[6]
(0.79 ± 0.25) kJ/m^2	Nacre without the calcitic layer under wet conditions (7)	Single edge notched three-point bending; notch in *yz*-plane; crack travels in *y*-dir.; load ⊥ *z*-axis		Genus: *Pinctada* (bivalve!)	[6]
(0.44 ± 0.14) kJ/m^2	Nacre without the calcitic layer under dry conditions (11)	Single edge notched three-point bending; notch in *yz*-plane; crack travels in *z*-dir.; load ∥ *z*-axis	Crack propagation allowed until load dropped to zero; work of fracture calculated from the whole area under the force-displacement curve; span-to-depth ratio 4	Genus: *Pinctada* (bivalve!)	[6]
(1.03 ± 0.27) kJ/m^2	Nacre without the calcitic layer under wet conditions (12)	Single edge notched three-point bending; notch in *yz*-plane; crack travels in *z*-dir.; load ∥ *z*-axis		Genus: *Pinctada* (bivalve!)	[6]
(0.25 ± 0.07) kJ/m^2	Nacre without the calcitic layer under dry conditions (9)	Single edge notched three-point bending, notch in *yz*-plane; crack travels in *y*-dir.; load ⊥ *z*-axis		Genus: *Pinctada* (bivalve!)	[6]
(0.55 ± 0.17) kJ/m^2	Nacre without the calcitic layer under wet conditions (11)	Single edge notched three-point bending, notch in *yz*-plane; crack travels in *y*-dir.; load ⊥ *z*-axis		Genus: *Pinctada* (bivalve!)	[6]

"Mode I" loading. In this case the applied tensile stress to the specimen is perpendicular to the crack plane. K_c denotes the critical stress intensity factor, which can be used to determine the critical conditions in terms of remote stress and crack size leading to failure of the material.

The two parameters that can classify the crack resistance of linear elastic solids are uniquely related by

$$G = \begin{cases} \dfrac{K_1^2}{E} & \text{plane stress} \\ \dfrac{K_1^2\left(1-\nu^2\right)}{E} & \text{plane strain} \end{cases} \tag{6}$$

If the material shows nonlinear behaviour other parameters are more appropriate for judging the resistance of a solid to crack propagation. One possibility is the measurement of the crack-tip-opening displacement (CTOD). Due to plastic deformation an initially sharp

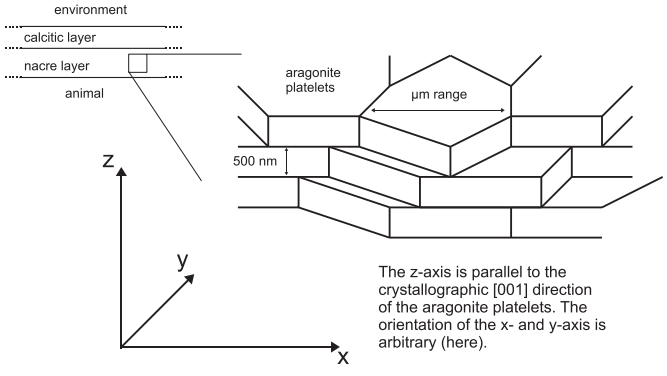

Fig. 12. Directional indicators used in Table 4.

crack tip blunts under load and therefore reduces the peak stresses at the tip. The CTOD can be related to the nonlinear energy release rate *J*. The nonlinear energy release rate can be defined in similar manner to Eq. (2). Nevertheless measurement and computation of *J* are different compared to the linear case (see e.g. [102]).

If we take a look at Fig. 11 it is interesting to notice that the fracture toughness of mollusc shells is at least one to two orders of magnitude higher compared to calcite although the mineral fraction is in the order of 95 wt.%. Comparing the toughness range for shells with those of man-made materials as shown in Table 3 it can be stated that the natural composite is almost as tough as some engineering ceramics, engineering polymers and even some alloys.

Table 4 summarizes measured mechanical properties of gastropod nacre and gastropod shells respectively. It has to be pointed out that different shell-forming animals build up different shell structures with varying mechanical properties [105–108]. In this review we focus on the columnar nacre of gastropod shells.

The mechanical properties of nacre depend strongly on the orientation of the specimen during the experimental investigations — it is an anisotropic material. Fig. 12 explains the terms used for different nacre orientations used in Table 4.

Considering Fig. 13A it is obvious that nacre exhibits in the initial linear regime an elastic modulus – in the order of magnitude of 100 GPa – comparable to that of the mineral phase. It has to be added that the mechanical properties of aragonite are anisotropic with considerable differences in the elastic moduli (see e.g. [109,110]).

But in contrast to aragonite (and dry nacre) wet nacre shows a distinctive nonlinear regime before failure at a strain in the order of magnitude of 0.01 (tensile failure strain). The ultimate tensile strength is around 100 MPa and seems to be lower for hydrated nacre.

As indicated previously a rising *R*-curve – as in the case of nacre (Fig. 13B) – can be associated with extrinsic toughening mechanisms. Some of them will be discussed in the following section.

Unfortunately we were not able to find references to fracture toughness values for aragonite — not even in articles dealing with toughness of nacre. But at least we can provide an estimation of required fracture energy from surface energy values. De Leeuw and Parker [111] performed atomistic simulation studies to calculate the energies of different aragonite surfaces. Since the calculated surface energies do not exceed 2 J/m^2 and the required fracture energy of a crystal is lowered due to flaws this value can be regarded as an estimation of the upper boundary for a perfect crystal. Barthelat et al. [112] claim a maximum of about 10 J/m^2 for the toughness of an aragonite mineral. A fracture toughness value of (0.39 ± 0.12) MPa$\sqrt{\text{m}}$ for calcite for one distinct surface/load direction can be found in [113]. This value might serve as a reference point for the order of the toughness values that can be expected for aragonite.

In this context the (at least) one hundred fold increase in fracture energy of nacre containing approx. 95 wt.% of the brittle mineral is remarkable.

The organic layer seems not to be topic of many investigations. For attempts to characterise the mechanical properties of the interface between the platelets consult Meyers [114] and Katti [115].

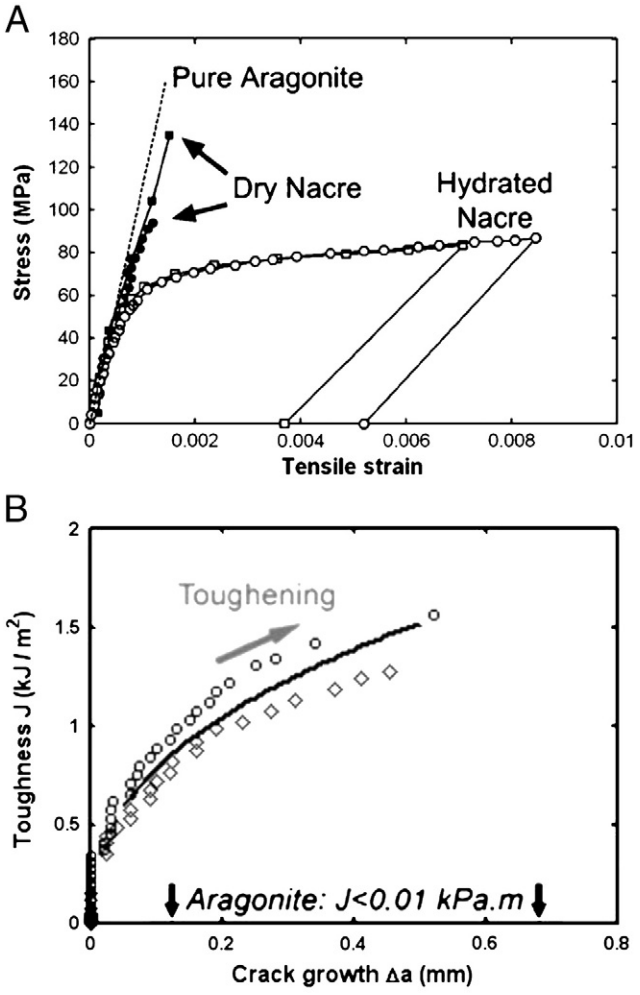

Fig. 13. A. Stress–strain curve for aragonite and nacre (hydrated and dry). B. Rising *R*-curve of nacre indicates extrinsic toughening mechanisms.
With kind permission from *Springer Science + Business Media: Experimental Mechanics, An Experimental Investigation of Deformation and Fracture of Nacre-Mother of Pearl, Vol. 47, 2007, 311–324, F. Barthelat and H.D. Espinosa, Figs. 5a and 16.*

3.3.3. Toughening mechanisms in nacre

The central question to be answered is: how can a biological composite like nacre with its characteristic columnar brick-and-mortar structure made of stiff and brittle aragonite as well as ductile and weak organic layer achieve strength and resistance against crack propagation?

Considering briefly the elastic modulus of a composite material like nacre there are two limiting models (see [6]). The upper boundary is given by the Voigt model, which assumes that the mineral and organic phase undergo the same strain. Let Φ be the volume fraction of the mineral. E_m and E_p are the elastic moduli of the mineral and organic layer respectively. Then the elastic modulus of the composite can be stated as

$$E_c = \Phi E_m + (1-\Phi)E_p \tag{7}$$

The lower boundary can be estimated from the Reuss model, which assumes that the components experience the same stress upon loading. The elastic modulus of the composite then reads

$$\frac{1}{E_c} = \frac{\Phi}{E_m} + \frac{(1-\Phi)}{E_p} \tag{8}$$

Applying the tension–shear model (Fig. 14) to biocomposites Gao and co-workers [116] give an estimation for the elastic modulus

$$\frac{1}{E_c} = \frac{4(1-\Phi)}{G_p \Phi^2 \kappa^2} + \frac{1}{\Phi E_m} \tag{9}$$

G_p and κ denote the shear modulus of the organic layer and the platelet aspect ratio (longer dimension divided by shorter dimension) respectively. It is expected that the shear modulus of the polymer is clearly lower than the elastic modulus of the mineral. Consequently a high aspect ratio is required to avoid a dominating influence of the weak organic layer on the composites elastic modulus. The role of the platelet aspect ratio in toughness is discussed below.

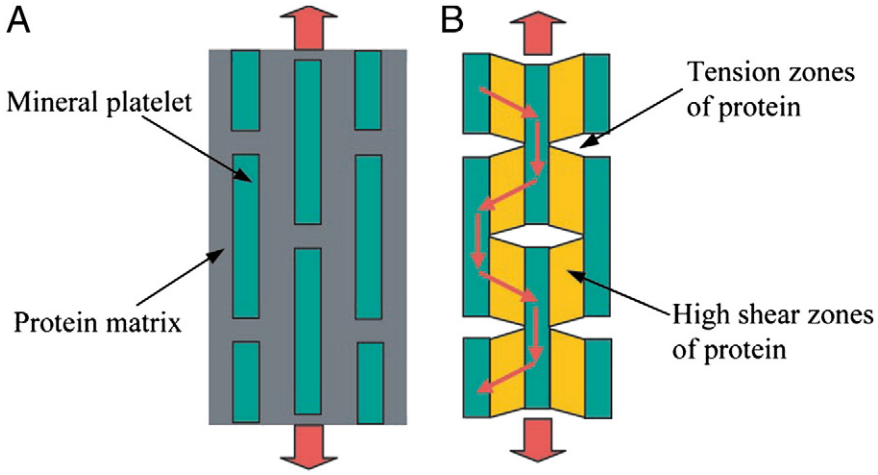

Fig. 14. A. Mineral platelets orderly embedded in an organic matrix. B. The load is transferred by shearing the organic layer during stress (parallel to the platelets). The mineral platelets carry most of the load applied to the composite.
From *H. Gao, B. Ji, I.L. Jäger, P. Fratzl, Materials become insensitive to flaws at nanoscale: Lessons from nature, Proceedings of the National Academy of Sciences U.S.A., Vol. 100, pp.5597–5600 (2003).* Copyright (2003) National Academy of Sciences, U.S.A.

While investigating the surface of fractured specimens Currey [117] deduced ideas for toughening mechanisms. At first during the process of fracture new surfaces are formed which requires at least the surface energy of the fractured material.

Due to the brick–mortar structure a crack running perpendicular to the shell surface (perpendicular to the tablets) often travels around single platelets thus increasing the actual crack path length. This means that the "pull-out" of mineral platelets is preferred instead of mineral fracture and thus increasing the required work of fracture. But if the platelets just get pulled out of the organic then the weak organic would determine the mechanical properties of nacre. Consequently there must be a load distribution mechanism (see following paragraphs).

If in the case described previously the tensile load is applied parallel to the mineral platelets then the crack propagates sometimes in the organic layer parallel to the tensile forces (e.g. [118]).

This is an unfavourable propagation direction in the following sense. It was shown ([118]) that if a crack travels perpendicular to the applied load in a solid and approaches a plane of weakness (in the context discussed here an organic interface) the crack starts travelling in the plane of weakness parallel to the applied load. The authors point out that the elastic energy required for crack extension parallel to the load increases less steep with crack length than perpendicular to the load. In nacre additionally a separation of adjacent platelets causes crack blunting and therefore reduces stress at the crack tip. Thus the microstructure of nacre under appropriate load conditions leads to toughening.

Analysing the surfaces of fractured specimens Jackson et al. [6] became aware of organic matrix threads that seemed to bridge stress generated gaps between platelets. The authors even noticed "globules" in the organic matrix that could "untie" during the bridging of gaps.

Jackson points out that the mechanical toughness of dry nacre is worse than the toughness of wet nacre. Since water strongly influences the condition of the organic layer it has to play an important role in toughness of nacre. If one assumes that proteins of the organic matrix are responsible for the platelet–matrix–platelet connection and therefore are important for the material toughness then a drying of the organic matrix removes the "natural water environment" of the proteins. This could lead to protein miss-folding and loss of protein side chain mobility and consequently the decreasing interaction capabilities of proteins.

In the course of the past years other ideas were added or refined (for an overview see [119]).

Nevertheless the essential principles to maximize the work of fracture remain: increase of the crack surface, resistance to platelet sliding, platelet interlocking, reduction of peak stresses especially in notches and use of stretchy molecules for crack bridging.

Smith and co-workers [61] were able to show that force-extension curves of molecules from the organic layer of a freshly cleaved nacre surface show a sawtooth-like pattern. This indicates the unfolding of protein domains, opening of intra-chain loops or rupture of inter-chain bonds. Upon relaxation of the stretched molecules from the organic layer no "refolding" into the former arrangement was observed. Therefore a considerable amount of work is dissipated during the extension. This molecular feature might contribute to the inelastic deformation prior to fracture, energy dissipation and efficient crack bridging.

Barthelat et al. [112] calculated that – although the crack-bridging mechanism is evident in experimental observations – its contribution to the measured toughness is small compared to energy dissipation in an inelastic deformation zone emerging around a crack tip (see below).

Ji and Gao appended [120] that the viscoelastic properties of the biocomposite are beneficial to fracture energy dissipation. If the elastic modulus decreases during loading – this can occur if the initially entangled polymers in the organic layer rearrange in the course of loading – a viscous energy dissipation zone is formed around the tip of a propagating crack. This mechanism increases the required fracture energy and can even stop crack propagation by reducing the stress concentration.

Several models have been proposed to explain the load transfer and stress distribution between the platelets inside the composite during deformations of specimens. This is an essential process to form an energy dissipative zone around an advancing crack.

First it can be stated that the organic layer is not capable to resist large stresses without large plastic deformation and/or rupture.

One possibility to transfer load from the weak organic to the more tough platelets is simply by shear. This requires that (at least some) organic molecules are connected to the platelets and are able to sustain the shear stress. On the other hand the platelets must resist the tensile stresses without fracture. To ensure the fracture resistance of the brittle mineral the dimension of the platelets seem to play an important role. Currey [117] suggested that the thin (height of approximately 0.5 μm) aragonite platelets of nacre are a further source of its toughness. Gao et al. [26] estimated a critical length scale from the Griffith crack criterion.

In linear elastic fracture mechanics from the Griffith relation

$$\sigma_m^f = \alpha\sqrt{\frac{E_m\gamma}{h}} \tag{10}$$

the fracture stress of a material (here the mineral platelet) σ_m^f that contains a crack of length h can be estimated if the elastic modulus E_m and the surface energy γ of the solid are known. The factor α describes the crack geometry. The crack length in the solid cannot be larger than the solids dimension (here the height) so the crack length can be identified with the mineral platelet height.

It turns out that if typical values for the surface energy, elastic modulus and theoretical tensile strength are inserted in Eq. (10) then a nanometer thick mineral platelet shows a tensile strength close to the limiting theoretical value.

As well as the mineral platelet height, Gao and co-workers found that the aspect ratio of the platelets is optimized in natural composites. The optimal aspect ratio is given by

$$\kappa = \frac{\text{longer dimension (width or length)}}{\text{shorter dimension (height)}} = \frac{\sigma_m^f}{\tau_p^f} \propto \frac{1}{\sqrt{h}} \tag{11}$$

where σ_m^f is given by Eq. (10) and τ_p^f is the shear strength of the protein layer. In Eq. (11) the simultaneous failure of the protein layer and the mineral is assumed. The authors estimated an optimal aspect ratio for nacre of approximately 10.

This approach has been criticised e.g. by Ballarini et al. [34]. First the authors point out that in Gao's model no plasticity and/or other energy dissipating mechanisms are included. They further question the validity of the Griffith crack criterion (10) at theoretical stresses. With an "approximate bond force model of the Lennard–Jones type" where they state the stress to separate two atoms of a material by a distance x as

$$\sigma(x) = \frac{E}{m-n}\left(\frac{b}{x}\right)^n - \left(\frac{b}{x}\right)^m \tag{12}$$

where b is the equilibrium lattice spacing of atoms and n, m are material constants (e.g. $n=2$, $m=10$ for ionic solids). From Eq. (12) they could derive a relation between the theoretical strength and Young's modulus

$$\frac{\sigma_{th}}{E} = \frac{1}{m}\left(\frac{n}{m}\right)^{\frac{n}{m-n}} \tag{13}$$

In combination with Eq. (10) they estimated the crack length where the fracture strength equals the theoretical strength to be approximately eight times the equilibrium lattice spacing (ionic solid). This is clearly below the postulated 30 nm of Gao et al. So due to Ballarini et al. every crack with length above $\approx 8b$ should weaken a solid. The last-mentioned authors stress that the toughening mechanisms for the whole shell of *Strombus gigas* are crack arrest at the interfaces between cross-lamellar layers of the shell and separation of inner-lamellar mineral layers (see Ballarini et al. for details). The microstructural hierarchy of the whole shell is supposed to be responsible for the toughness of the biological material rather than nanoscale minerals.

Another possibility of distributing the applied stress in a piece of nacre is by platelet interlocking mechanisms (Figs. 15–17). Several interlocking mechanisms have been proposed discussed in the following.

During mechanical testing several experimenters (e.g. [33]) noticed an inelastic deformation zone at a tip of a crack. If the crack notch is orientated perpendicular to the mineral tablet face then the inelastic deformation zone arises from tablet separations (sometimes denoted as "dilatation bands"). The authors note similarities to phase transformation-toughening mechanisms (e.g. [121]).

Wang and co-workers [33] and Evans and co-workers [122] emphasize the importance of inelastic deformations responsible for peak stress reduction at stress concentration sites (see e.g. [123,124]) improving fracture resistance. Some characteristics of the aforemen-

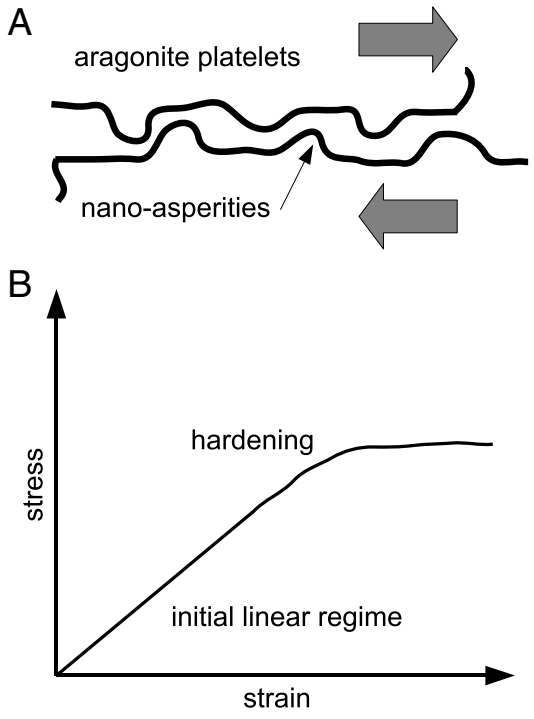

Fig. 15. A. Sketch of two aragonite platelets with nanoasperities sliding over each other. B. The stress–strain curve of nacre shows strain-hardening.

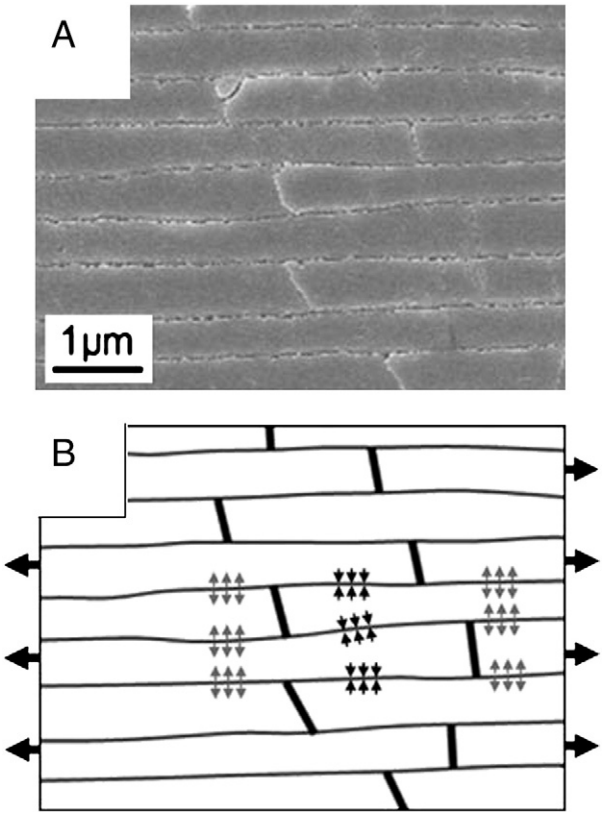

Fig. 16. A. "Waviness" of aragonite platelets in nacre. B. Interlocking of aragonite platelets.
With kind permission from *Springer Science + Business Media: Experimental Mechanics, An Experimental Investigation of Deformation and Fracture of Nacre-Mother of Pearl, Vol. 47, 2007, 311–324, F. Barthelat and H.D. Espinosa, Fig. 8.*

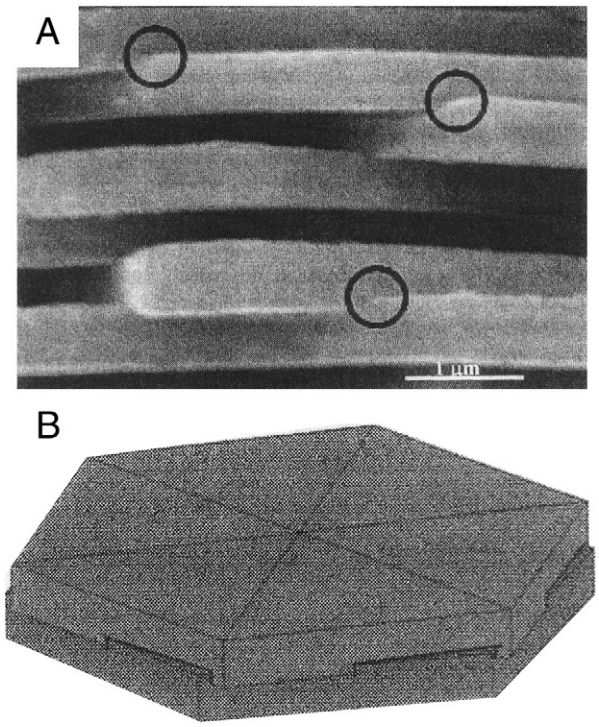

Fig. 17. A. Image of interlocked aragonite platelets. B. 3-dimensional model of interlocked platelets.
From *K.S Katti, D.R. Katti, S.M. Pradhan, A. Bhosle, Platelet interlocks are the key to toughness and strength in nacre, Journal of Materials Research, Vol. 20, pp. 1097–1100 (2005)*. Reprinted with kind permission of the authors and Materials Research Society.

tioned dilatation bands are that they form normal to the applied load if the elastic strain regime is left and that the formation of gaps between platelets is possible through platelet sliding.

Evans and co-workers [122] and Wang and co-workers [33] imaged nanoscale asperities ("nanoasperities") on the mineral platelets (Fig. 15A shows a sketch; for SEM images consult [33] and [122]) and developed a model how these small features provide resistance to platelet sliding and enable strain-hardening. Considering Fig. 15B the stress-strain curve starts with an initial elastic regime in which the organic layer and mineral bridges can bear the load. In their model the following strain-hardening domain is explained by nanoasperities that climb over each other. If the asperities of two adjacent platelets shear over each other and get into mechanical contact the platelets repel each other perpendicular to the shear direction. This separation leads to internal compression increasing the required force for further shearing. If the applied load reaches a threshold value the deformation continues without any additional strain-hardening. This value is adjusted so that the formation of multiple dilatation bands is favoured over platelet fracture.

In this model the mechanical purpose of the organic layer is to lubricate the interfaces of the shearing plates and to distribute the stress between the dilatation bands.

Barthelat and colleagues take the opinion [125] that the nanoasperities can only provide a shear resistance over smaller sliding distances than observed in experiments. They proposed an alternative model for the observed large inelastic deformation of nacre and the hardening mechanism [112,126].

While investigating cross sections of nacre they noticed a "tablet waviness" (Fig. 16A). The authors argued that the unfolding of the biopolymer(s), which occurs roughly at constant load, and that nanoasperities, for reasons given previously, cannot provide the observed hardening. Instead they propose a progressive interlocking of the wavy platelets during sliding as the source of hardening and deformation spreading (Fig. 16B). This works in principle the same way as described previously for the asperties. A macroscopic model of nacre with interlocking of adjacent nacre platelets is described in [96].

Katti and co-workers [127] took images of the fracture surface of nacre and detected "interlocks" of stacked platelets (Fig. 17). Two adjacent platelets that are stacked extend into each other. Simulations show that if load is applied parallel to the platelets progressive failure of the interlocks causes strain hardening and explain the observed strength and strain values.

The load distribution and hardening models introduced so far are applicable for a specimen in tension. If nacre is subjected to compressive loads another energy dissipation mechanism occurs. Menig et al. [128] observed plastic microbuckling during compression of shell specimens parallel to the tablets (Fig. 18). Since the platelets are not oriented exactly parallel to the applied load the layers shear against each other if the load reaches a threshold. This plastic deformation reduces the stored strain energy.

We assume that this compilation of information regarding the toughening mechanisms of nacre is not complete but nevertheless contains the most important features. Additionally we neglected the whole complex of computational approaches to the problem due to the fact that the simulations rely on the accuracy of the experimental input values.

4. Growth

In light of the iridescent beauty of nacre, its outstanding mechanical properties, and its highly ordered structure (described in the previous sections), a detailed understanding of the formation process is obviously of great interest. An understanding of how nacre forms could provide inspiration for the creation of new types of biomimetic engineering materials, either formed or repaired by the use of self-organising processes.

Furthermore, nacre could stand as a model system for biomineralisation: principles valid for nacre growth may be common for $CaCO_3$ biomineralisation, or even turn out to be general principles of biomineralisation itself. This is justified by the relatively simple and organised structure and its early occurrence in the history of life: nacre was found in fossil records of the earliest shell-forming molluscs [129].

It must be pointed out that many aspects of nacre growth are not conclusively elucidated and are the object of ongoing research. This especially applies to the detailed mechanisms of how the organisms control nucleation and growth as well as the assembly of the organic matrix.

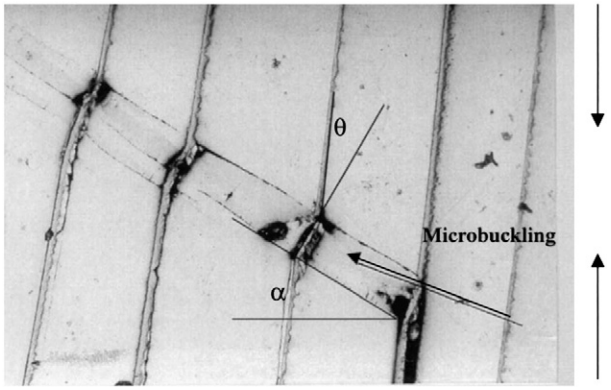

Fig. 18. Microbuckling in nacre after compressive load parallel to the *xy*-plane of the platelets [128].
This article was published in *Acta Materialia, Vol. 48, R. Menig, M.H. Meyers, M.A. Meyers, K.S. Vecchio, Quasi-static and dynamic mechanical response of Haliotis rufescens (abalone) shells, 2383–2398*, Copyright Elsevier (2000).

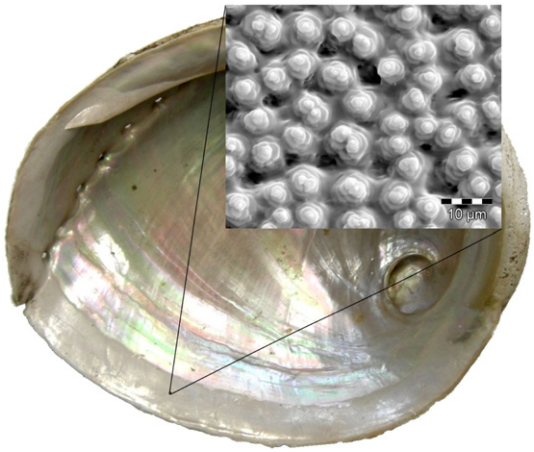

Fig. 19. Photograph of the nacreous inner side of a shell of the marine snail *Haliotis laevigata* (greenlip abalone). The diameter of an adult greenlip abalone shell is approximately 15 cm. Shell growth takes place at the outer edge of the shell, the region of nacre growth is visible with the naked eye as a region of dull appearance. The inset shows a SEM micrograph of the nacre growth region with stacked aragonite platelets. Remnants of the organic matrix can be observed between the stacks.

4.1. Growth morphology

In abalone shells, the location of nacre growth is often visible with the naked eye as a region of dull appearance located at the border of the inner side of the shell (Fig. 19). Scanning electron micrographs of this area (Fig. 19, inset) reveal the structure of gastropod nacre growth to be platelets of aragonite crystals that stack up into pyramidal shapes [5,130,131]. Lateral growth of the crystals proceeds until the crystal layer is continuous, forming the finalised nacreous layer (Fig. 20). This mode of nacre deposition is different from that which occurs in bivalves, where aragonite crystals are deposited layer by layer [132]. The pyramidal growth morphology of gastropod nacre seems to provide a faster growth rate than that of bivalves, since several platelets can grow simultaneously. This is thought to compensate for the small growth area in gastropods compared to bivalves, where almost the entire inner side is a growth surface [131,133]. Although the presence of an organic component in finalised nacre was identified decades ago (in older articles sometimes referred to as 'conchiolin'; referred to here as 'organic matrix') [134,135], its structure before and during growth was unclear.

After development of suitable preparation and investigation methods, pioneering SEM imaging of the nacre growth region revealed the presence of well-organised organic sheets prior to complete mineralisation [130,131]. Using transmission electron microscopy of ultramicrotome sections, it was possible to observe the structure of the growth region in great detail. Initial observations were made on bivalve nacre around 1970 [132,136,137]. Investigations on gastropod species by Nakahara and colleagues followed about 10 years later [3,5].

Fig. 20C shows a typical TEM micrograph of growing gastropod nacre. Prior to nucleation of the first aragonite tablet, a part of the organic matrix forms roughly even-spaced interlamellar sheets, which are then filled by laterally growing aragonite crystals. On top of the aragonite stack, several sheets lie more densely packed (denoted 'SS' in Fig. 20C). These stacked sheets are thought to form a protective shield of the growth area against distortions caused by the relatively mobile gastropods, as well as provide a reservoir for the further vertical growth of nacre [3,131].

The identification of organic sheets formed prior to mineral deposition was interpreted as a confirmation of the 'compartment theory', which postulates that nucleation and growth of the mineral phase occur in pre-formed organic compartments [3,5,132].

4.2. Cells of the mantle epithelium control the mineral deposition

Secretory epithelial cells of the mantle are responsible for the inductions of the different stages of shell formation. These cells are located at the dorsal (shell side) surface of the mantle of the animal, which forms a closed space between the organism and its shell [12,132]. This so-called extrapallial space (*pallium*, Latin for cloak/mantle) is filled with extrapallial fluid, which is supposed to contain the required inorganic ions [89] as well as the complex organic matrix [132,133,136]. It is a central assumption of shell biomineralisation that the type of secreted organic matrix plays a major role in defining the type of shell layer formed [138]. Fig. 20A shows a schematic vertical cross fracture surface of shell growth in abalone.

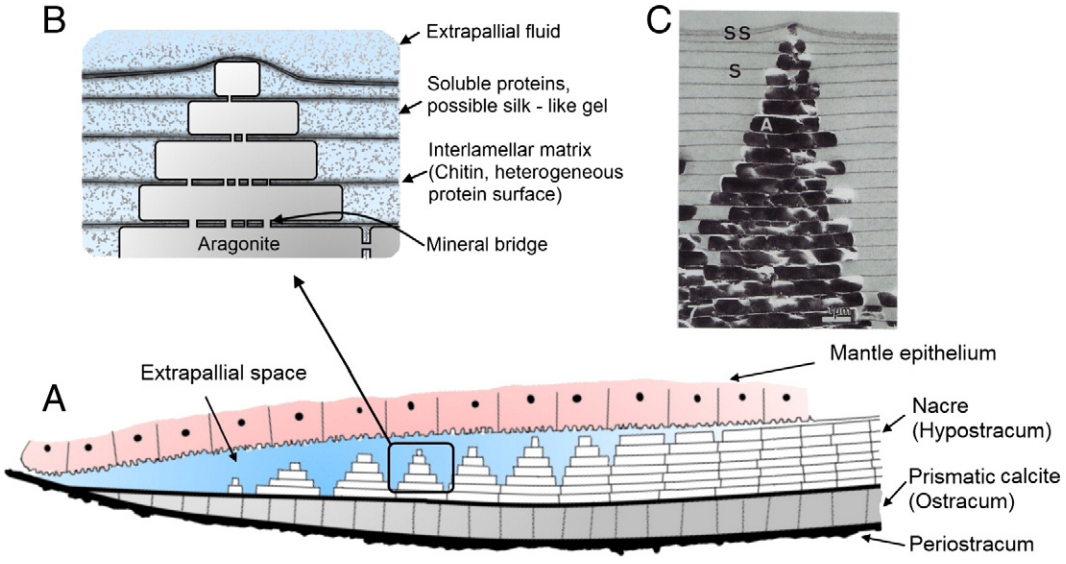

Fig. 20. A. Schematic vertical cross section (not to scale) of the outer mantle edge and the growing shell in *Haliotis*. The cells of the mantle epithelium control the composition of the extrapallial fluid. The different shell layers grow by a self-organisation process. Initially (left), the organic Periostracum is deposited, followed by the growth of prismatic calcite and nacre. Intermediate shell layers have been omitted for simplicity. B. Scheme of nacre growth. The mineralisation takes place in pockets of the interlamellar matrix soaked with ions, soluble matrix proteins and presumably a silk-like gel. C. TEM micrograph of a thin cut of growing gastropod nacre (species *Tegula pfeifferi*, lead citrate single stain). ('A') Aragonite crystal stack. ('S') organic sheet. ('SS') Surface sheets [133]. With kind permission of Springer Science + Business Media.

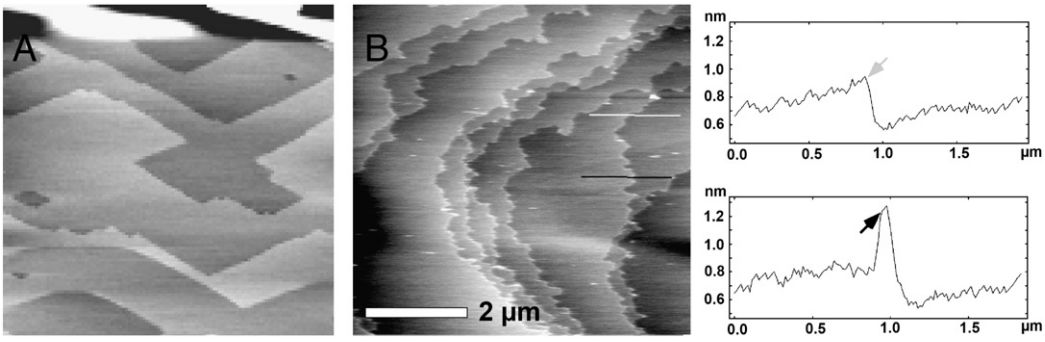

Fig. 21. A. AFM image of a calcite surface in deionized water. The different gray levels represent monomolecular layers of the calcite [441] surface. B. AFM image of a calcite surface in the presence of the small 4.8 kDa nacre protein Perlinhibin (in 7.5 mM $CaCl_2$). The protein binds to steps and kinks of the calcite crystal and locally prevents dissolution of the crystal at the binding site. The resulting surface has a fringed appearance due to bound proteins which are visible as small white spots. The line plots a the right side compare the height profile over a step without (gray) and with (black) bound protein. Without protein the typical step height for calcite of about 0.35 nm is observed, whereas with bound Perlinhibin the step height is increased to 0.7 nm.
Reprinted from *K. Mann, F. Siedler, L. Treccani, F. Heinemann, and M. Fritz, Perlinhibin, a cysteine-, histidine-, and arginine-rich miniprotein from abalone (Haliotis laevigata) nacre, inhibits in vitro calcium carbonate crystallization, Biophysical Journal 93 (2007) 1246–1254.* Reprinted with the kind permission of the authors and Elsevier.

The relationship between organic matrix secretion by the cells of the mantle epithelium and mineral deposition can be studied *in vivo* by inserting inorganic substrates (e.g., glass slides) between the shell and the mantle of the animal [12,17,21,139,140]. This so-called flat pearl technique [17] triggers the formation of new shell layers on a flat surface. The newly formed overgrowth resembles the arrangement of the native shell in spatial and temporal order (organic sheet followed by calcite and nacreous layers), and is used to investigate the different stages of shell formation. The organism's ability to restart the sequence of shell deposition after sensing an inserted surface indicates that individual cells of the mantle epithelium are able to secrete different types of organic matrix. Sharp transitions between the different shell layers were observed, showing the strict control that the organism has over mineral formation [12]. Another investigation, using in situ hybridisation of mRNA coding for two proteins of either the prismatic calcite or the nacreous layer in the bivalve *Pinctada fucata*, revealed that cells at the outer edge of the mantle epithelium secrete proteins necessary for the calcite layer formation and cells located at the inside secrete proteins necessary for nacre formation [49].

Possibly due to the small amount of extrapallial fluid and complicated experimental access, only two studies focusing on the inorganic composition of the extrapallial fluid have been published to date [89,141]. In the investigated marine bivalves (no gastropods and no freshwater species were investigated) the inorganic composition was similar but not equal to sea water [89] and the haemolymph [142] (Table 5). In nearly all results, the concentration of inorganic carbon (CO_2 or HCO_3^-) in the extrapallial fluid was higher than in sea water; calcium was always slightly elevated. The $CaCO_3$ supersaturation level of the extrapallial fluid deviated greatly due to the difference of reported pH values, which mainly control supersaturation by the pH-dependent distribution of the carbonate species. The values reported by Wada and Fujinuki [141] represent a strong supersaturation, whereas the values reported by Crenshaw [89] do not. The high magnesium concentration of the extrapallial fluid is of interest: at about 50–60 mM it is 5–6 times higher than the calcium concentration. In precipitation assays, such high magnesium/calcium fractions were found to favour aragonite growth [143] and to delay the onset of precipitation [144]. Nevertheless, it seems unlikely that shell growth depends on the detailed ionic composition of the extrapallial fluid, considering the organism's ability to induce the growth of different shell layers containing different $CaCO_3$ polymorphs in close proximity simply by changing the type of organic matrix secreted.

4.3. Pores, mineral bridges, domains and implications for nacre growth

Although the existence of defined organic compartments prior to mineral deposition was generally accepted after publication of the first TEM images of ultramicrotome thin sections of growing nacre in gastropods [3], it was not known whether each platelet was nucleated independently or if the platelets were connected by mineral bridges through pores in the interlamellar matrix sheets. Pores had been observed by electron microscopy (SEM and TEM) in early studies on the interlamellar sheets on bivalves [132,136] and gastropods [5,133]. However, due to the sensitivity of the organic material, the possibility remained that these structures might also be preparation or imaging artefacts [21].

Investigations of the interlamellar sheet of demineralised flat pearls by atomic force microscopy and scanning ion conductance microscopy verified the existence of pores in the interlamellar matrix in an aqueous solution. It was found that the matrix sheets are pervaded with pores of 5–50 nm in diameter and a density of about 50–100 pores/µm^2. These pores were shown to be conductive for ions, but, due to their size, it was assumed that they also allowed the diffusion of soluble proteins. The possibility of mineral growth through these pores, forming so called mineral bridges connecting adjacent aragonite platelets, was also suggested [21].

Schäffer and colleagues produced the first TEM images of inorganic material crossing the pores inside the organic matrix in 1997 [21], but the authors noted that the image quality was not sufficient to prove the existence of mineral bridges conclusively. In the following years,

Table 5
Range of measurements of the inorganic composition of the extrapallial fluid of several marine bivalve species compared with sea water and the haemolymph of *Strombus gigas* (a marine gastropod). Analysis 1 represents the range of values from 3 species [89], analysis 2 represents the range of values from 4 species [141].

Ion	Analysis 1 [89]	Analysis 2 [141]	Haemolymph [142]	Sea water [89]
Na^+ (mM)	441–444	422.8–431.5	495.9	427
K^+ (mM)	9.4–9.6	9.6–12.7	10.9	9.0
Ca^{2+} (mM)	10.65–11.6	9.5–9.9	11.3	9.3
Mg^{2+} (mM)	57–60	48.2–50.7	58.28	53
Cl^- (mM)	472–480	520.1–552.6	557.8	496
SO_4^{2-} (mM)	46.1–47.3	26.2–33.3	20.48	51.1
CO_2 (mM)	4.2–5.2	–	–	2.5
HCO_3^- (mM)	–	2.4–5.2	10.16	–
pH-value	7.33–7.41	8.4–8.53	7.91	7.91

several further studies reported the discovery of connections between stacked platelets and provided TEM images of good quality [32,125,140,145].

Synchrotron spectromicroscopy of vertical nacre cross sections demonstrated that the *a*- and *b*-axis of up to 40 platelets are parallel oriented in the abalone *Haliotis rufescens*. This parallel orientation of platelets was for the most part along the vertical direction, but laterally parallel oriented platelets were also observed [146], possibly due to growth via mineral bridges in the lateral direction. These findings are supported by recent studies using high resolution TEM on stacked aragonite platelets of *Haliotis laevigata* [32] and *Pinctada fucata* [147], which show that the crystal lattice is continuous over mineral bridges, resulting in a transfer of the platelet orientation.

The existence of domains of platelets with constant orientation led to conclusions about the growth mechanism [146]. Nucleation events of aragonite platelets occur at randomly distributed sites on or in the preformed organic matrix. These nucleated aragonite crystals then grow in a vertical and lateral direction through pores in the organic matrix until they come into close contact with neighbouring crystals to form the finalised material (see also Fig. 5).

4.4. Formation of the interlamellar matrix

To date, the processes that form the interlamellar matrix inside the extrapallial space are only partially understood. Since the interlamellar matrix itself has a hierarchical construction [129], a full formation model of the interlamellar organic matrix should comprise all structural levels, beginning with the synthesis of the individual components and ending with the modalities that produce the assembly of evenly spaced interlamellar matrix layers.

A protein involved in chitin synthesis by the cells of the mantle epithelium was recently described by Weiss et al. [148]. The authors report the cDNA of a chitin synthase (Ar-CS1) for the bivalve species *Atrina rigida* and a homologous gene (Mg-CS1) for the bivalve *Mytilus galloprovincialis*. The reported chitin synthase is a transmembrane protein containing motifs similar to insect chitin synthases. In addition, it contains an intracellular myosin head domain, supposing a connection with the cytoskeleton [148]. After secretion into the extrapallial space, the chitin possibly crystallises with neighboring chitin polymer chains to β-chitin fibrils [129].

Chitin of the bivalve *M. galloprovincialis* was reported to be covalently modified with additional hydrophobic side-groups, apparently resulting in an amphiphilic property of the modified chitin [149]. This amphiphilic property could be an important driving force for self-organisation, resulting in the observed layered organic sheets. The modified chitin fraction might form the interface between the chitin core and the interlamellar matrix surface, which is in contact with the proposed hydrophobic silk-like gel [49,150–153] between the interlamellar layers.[2]

In 2009, Checa et al. showed TEM images of extracellular vesicles, fusing with the surface of the interlamellar matrix sheets at the mantle side of gastropods [154]. Already in the TEM images by Nakahara et al. these vesicles are perceivable to some extent (above 'SS' layer, right side in Fig. 20C). In the new images of higher resolution, the vesicles are hollow and have a two-layer appearance. Surprisingly, the surface sheet itself ('SS' in Fig. 20C), which is formed by the layered vesicles, is apparently homogeneous. On the nacre side (below 'SS' sheets in Fig. 20C), interlamellar sheets were shown to detach from the surface sheet, a process that occurs simultaneously with the vertical penetration of the topmost aragonite crystal into the surface sheet. The reasons for this detachment from the homogeneous surface sheet are yet unknown, but result in a layered interlamellar matrix sheet (containing a chitin core and attached proteins). Possibly, the amphiphilic nature of a chitin fraction cited previously helps to separate the interlamellar sheets.

4.5. Control over mineral formation

In the last decades, the high degree of control that organisms have over the mineralisation process has attracted the attention of many researchers. The following aspects of mineralisation are especially noticeable:

- Polymorph control: aragonite is nucleated exclusively.
- Morphology control: the aragonite in nacre forms platelets of about 500 nm height and several μm in diameter, which is a strong deviation from the needle like geologic crystal habit.
- Orientation control: the *c*-axes of the aragonite platelets are oriented almost perpendicular to the interlamellar matrix.
- Inhibition: no uncontrolled nucleation inside the extrapallial space.
- Nucleation: to some extent newly nucleated crystals must form, although most crystals seem to grow via mineral bridges.
- Transport of required ions to the site of crystal growth.

Several models have been developed to explain various aspects of the mineral formation process. A future comprehensive model should integrate the formation mode of the interlamellar matrix sheets as well as the entire mineralisation process. It will likely include and combine components of the different hypotheses presented below.

4.5.1. Ionotropic model

Ion binding studies performed in the 1970s and early 1980s led to the conclusion that the soluble matrix is capable of selectively binding calcium in the presence of other ions [155] (see below for the present-day view). Greenfield et al. reported a calcium binding capacity of 0.67 μmol/mg of EDTA extracted soluble matrix from the nacre of the clam *Mercenaria mercenaria* [156], whereas Wheeler et al. determined a calcium binding value of approximately 23 μmol/mg of EDTA extracted soluble matrix of the oyster *Crassostrea virginica* [157]. Although these values differ quite radically, both express a very high number of calcium ions bound to one matrix macromolecule. Assuming, for example, 50 kDa for the average molecular mass of a matrix molecule, this yields 33 (0.67 μg/mg) or 1150 (23 μg/mg) bound calcium ions per macromolecule.

Early histochemical investigations of the interlamellar matrix revealed that a part of the EDTA extracted soluble matrix, which was previously shown to bind calcium, remains located at a central region under each platelet when performing demineralisation under protein fixing conditions (in the presence of 4% formaldehyde). This central region was identified as sulphur and acid mucopolysaccharide containing, as well as calcium binding [158]. Thus, at least some fraction of the 'soluble matrix' is attached to the interlamellar matrix before demineralization with EDTA.

These calcium binding properties and the presence of charged groups at the central region of the interlamellar matrix led to the proposal of the ionotropic model [159] as a hypothesis for the nucleation process in nacre [156,160]. It was stated that calcium-binding groups, e.g., anionic sulphated polysaccharides bound to proteins, locally attract calcium at a nucleation site by electrostatic accumulation. These ions would then re-attract their counter ions and so forth. Due to the increased local super saturation of $CaCO_3$, a crystallisation of $CaCO_3$ should occur. Since no perfect positioning of ions was assumed, it was also proposed that the initial nuclei could be amorphous, with a subsequent phase transformation to crystalline aragonite [156].

The reports of the calcium-binding properties were re-evaluated by Wheeler et al. in 1987. The team carefully investigated the influence

[2] To date, this silk-like component has not been reported for the gastropod species, but its presence seems likely due to the close relationship of the nacreous layers formed by the two classes.

of residual EDTA present in soluble matrix fractions on the results of calcium binding studies, and found that EDTA is very difficult to remove from matrix samples, since it interacts with matrix proteins. Calcium binding studies on EDTA-free samples showed no calcium binding, reversing previous results [161].

However, a more recent investigation, avoiding the artefacts induced by EDTA demineralisation, led to a partial confirmation of histochemical results obtained earlier by Crenshaw et al. [158] suggesting a tentative re-proposal of the ionotropic model. Nudelman et al. analysed the distribution of several chemical groups on the interlamellar matrix of nacre from the cephalopod *Nautilus pompilius* and the bivalve *Atrina rigida* by applying several staining methods [23]. A similar study was recently published for the gastropod *Haliotis rufescens* [22]. There was good evidence for a ring-shaped area with sulphate anions present on the interlamellar matrix of *Haliotis* and *Nautilus*. In addition, carboxylates could be stained in a central spot. In all species, a central region could be labelled with polyclonal antibodies against a soluble protein fraction extracted from nacre of *A. rigida* [162]. This protein fraction showed *in vitro* the capability to induce aragonite growth by using the ammonium carbonate method [19]. Therefore, it was assumed that the central spot has nucleating capabilities, for example, by highly ordered carboxylic groups of acidic proteins (see next section), whereas the negatively charged sulphate ring may help to locally supersaturate the environment by an ionotropic effect [23] (as already 1987 proposed by Addadi et al. [163]). Since the central spot is also the most likely region for the penetration of the first mineral bridges in a newly forming platelet, the ionotropic effect may also help to accumulate ions and foster further mineral growth of the newly growing platelet connected via a mineral bridge to an underlying platelet [22].

4.5.2. Epitaxy model of nucleation

One of the earliest (proposed in the 1960s) hypotheses for the nucleation of oriented aragonite was heteroepitaxy [130,131,136,137]. Heteroepitaxy (often shortened to the general term, epitaxy) in biomineralisation refers to a nucleation of the mineral on an organic matrix with chemical groups aligned so that they perfectly position the ions of the nucleating mineral phase. This represents a contrast to the ionotropic model, where a local supersaturation is assumed to favour nucleation. Initially the argument for the epitaxy model was based on the observation that the mineral grows on top of the surface of the organic matrix sheets [137].

The epitaxy model gained further support in 1980, when Weiner and Traub published results of X-ray diffraction measurements on the organic matrix of 10 nacre-forming species. Their interpretation of the diffraction patterns resulted in the description of an ordered protein component in the β-sheet conformation as a constituent of the interlamellar matrix (attributed to a silk-fibroin like protein due to results of amino acid analysis) as well as β-chitin in some cases. In one of the investigated species, *Nautilus repertus*, they found that the chitin fibrils and the β-sheet protein chains were oriented perpendicular to each other and aligned with the *a*- or *b*-axis of the aragonite platelets [45].

It was unclear whether or not this spatial relationship between mineral and organic matrix for *N. repertus* was typical for other species but not visible due to the large area investigated by XRD, thereby causing an averaging of differently oriented areas. By performing electron diffraction on a small area (about 6 μm^2) and consequently avoiding averaging effects on partially demineralised samples, Weiner et al. reported three years later that the protein chains were aligned along the aragonite *b*-axis [40] in all investigated species (gastropod, bivalve and cephalopod). This co-orientation of the mineral phase and a β-sheet protein component of the organic matrix made a strong case for the epitaxy model [40,41], since it is difficult to explain why the organic phase should align exactly with a specific crystal axis using other concepts.

Earlier findings by Weiner and Hood revealed that the soluble proteins contain a high fraction of aspartic acid. They proposed a hypothetical protein with β-sheet conformation and sequence asp–x–asp (with x representing glycine or serine). The distance between the carboxylic groups (6.95 Å) roughly matched Ca–Ca lattice spacing for aragonite and calcite (3.0 Å–6.5 Å) [18]. Considering that the soluble matrix originates to some extent from the interlamellar sheets, they proposed that the nucleation centers on the organic matrix were the previously reported asp–x–asp sequences, which align calcium ions by epitaxy [41].

Since the position of the calcium ions on the (001) faces of calcite and aragonite is almost identical, additional features to explain the selectivity between aragonite and calcite were required [164]. It must also be noted that to date, the main evidence for the epitaxy model is based on the results of the electron diffraction experiments from 1983 [40], which are supported by the finding of a central region of acidic proteins [22,23]. However, no similar XRD or electron diffraction results from other groups have yet been published, which show a co-orientation of ordered parts of the organic phase and the aragonite crystals.

4.5.3. Amorphous precursors

The idea that calcium carbonate in nacre and other biominerals does not crystallise directly from a solution but via a transient amorphous phase was briefly implied in older publications [136,156]. In recent years, the amorphous precursor hypothesis has been elaborated due to new experimental results and general considerations about the mineralisation process [152,165–168].

Investigations of different developmental stages of larval shells of the gastropod *Biomphlaria glabrata* indicated the involvement of amorphous calcium carbonate (ACC) in nacre formation before crystalline matter is present [169]. In a similar follow up study, [170], the authors confirmed the finding of ACC in larval shells. In comparing early stages of the shells, they found no X-ray diffraction signal (only a scattering contribution) although the shells already contained amounts of $CaCO_3$ (detected by thermogravimetry) as well as calcium (detected by electron spectroscopic imaging and extended X-ray absorption fine structure measurements). Furthermore, a recent study using SEM, IR-Spectroscopy and Raman imaging spectroscopy on shells of larval stages of two bivalve species yielded a similar result [171]. Hence, it is concluded that in the larval shell, amorphous calcium carbonate is a precursor stage which subsequently transforms into the more stable form aragonite [171], possibly according to Ostwald's empirical step rule [170,172].

ACC has also been reported as a transient phase in a number of other calcifying species (for an overview, see [165]). Since amorphous calcium carbonate is difficult to detect, especially when combined with a crystalline phase, some authors conclude that ACC precursors are a very common and previously overlooked feature of calcification [165,166,168].

A further argument for the involvement of ACC is the observation that minerals formed by controlled biomineralisation seem to adopt almost arbitrary shapes depending on their specific function. In contrast, geologically formed minerals usually adopt a specific crystal habit. Therefore, mechanisms must exist which allow the organism to control the geometry of the growing mineral. One way of achieving this could be the pre-filling of an organic mold (i.e. the organic matrix compartments present during nacre formation) with ACC [165,168], which is subsequently consumed by a growing crystalline phase nucleated on the matrix.

Finally, the transport of the ions and removal of solvent were taken as indicators for ACC precursors [152,168]. Addadi et al. considered the following [152]: an aragonite platelet of volume $10 \times 10 \times 0.5\ \mu m^3 = 0.5 \cdot 10^{-13}$ l contains about $1.5 \cdot 10^{-12}$ mol of $CaCO_3$. Due to the low solubility of aragonite (solubility product: $K_A = 10^{-8.336}\ M^2$ at 25 °C [84]) a more than 10^5 times higher volume of $CaCO_3$

containing solution would be required to dissolve and transport this amount of ions when assuming a saturated solution. According to the authors, "this clearly represents a logistical problem (…), both in transporting sufficient mineral (…) and removing large volumes of water." They proposed the possibility of mineral transport by ACC-containing vesicles [152]. However, it could be argued that nacre formation is relatively slow (typically 0.5 μm in the vertical direction per day [140]) and diffusion lengths are short, presumably allowing the animals to re-supply expended calcium and carbonate to the extrapallial fluid, which then might distribute due to diffusion. In the case of calcium (diffusion coefficient: $D \approx 3.73 \cdot 10^{-10}$ m^2/s [173]), assuming a diffusion length of 10 μm, the diffusion time would be less than one second.[3] Further, Addadi et al. assume a saturated $CaCO_3$ solution, but the exact saturation level of the extrapallial fluid is not well known (see Section 4.2) and supersaturation with respect to $CaCO_3$ is possible, which would lower the volume factor discussed previously. Stabilisation of the extrapallial fluid could be achieved by soluble nacre proteins, which are known to act as strong inhibitors of $CaCO_3$ nucleation and growth [157].

However, the existence of an amorphous precursor in nacre is a serious possibility, especially in light of the detection of ACC precursors in a number of calcifying species as well as in larval shells. But to date, there is no direct evidence proving the existence of ACC in the growing nacre of mature animals.

4.5.4. Control of growth by soluble nacre proteins

In all of the models discussed previously, the role of the soluble matrix is not clearly defined. Studies showed a strong inhibiting ability of the total soluble matrix [157]. With ongoing success in the purification and characterisation of nacre matrix proteins from *Haliotis*, a strong interaction with calcium carbonate *in vitro* was also found for most isolated nacre proteins. Some matrix proteins enhanced the crystal growth on calcite surfaces; (Perlucin [39,176], AP8 α, β [63,177]), whereas others were inhibitory on a calcite surface or in precipitation experiments (Perlwapin [58], Perlinhibin [59], AP7 and AP24 [62,177]).

The mechanism of crystal growth inhibition can be concluded from AFM studies on calcite surfaces in the presence of nacre proteins, e.g., Perlinhibin, which binds to monomolecular steps of calcite. Since crystal growth is most favorable on crystalline steps and kinks, a blocking of steps decreases the overall growing velocity. At moderate $CaCO_3$ supersaturations, this results in an inhibition of crystal growth, since dissolution and growth are competitive mechanisms. The protein binding sites can be clearly observed by a fringing of the calcite steps, which are locally blocked by proteins (Fig. 21) [59].

In the case of a preferred attachment of nacre proteins to specific crystal faces, this inhibitory capability would result in modified crystal growth velocities of the different crystal faces, finally resulting in crystals of strongly modified habit [138]. Due to the fact that the slowest-growing crystal faces govern the surfaces of a growing crystal, it is possible that the faces with strongest inhibition, e.g., due to protein binding to steps, represent the faces of the finalised crystal.

Elhadj et al., who found an increase of the calcite step propagation rate in AFM studies with artificial peptides at low concentrations, recently investigated the mechanism of crystal growth enhancement. This enhancing effect increased with both hydrophilicity and net negative charge of the peptide. The authors proposed that negatively charged and hydrophilic compounds increase the kinetics of ion attachment. Negatively charged compounds could help ions to attach to the crystal surface by the locally created electrostatic force gradient, whereas hydrophilic molecules might do so by restructuring water around the ions and at the crystal surface, both representing a barrier to ionic attachment [177].

A further effect of some of the soluble matrix proteins is the capacity to control the polymorph of forming $CaCO_3$ crystals [19,59,178,179]. By creating artificial substrates from β-chitin and silk fibroin, Falini et al. showed that proteins extracted from either the calcitic or aragonitic shell layers were capable of inducing their respective crystal polymorphs [19]. In a different study, polymorph selectivity for an isolated protein was found. After incubation of a calcite surface with a supersaturated $CaCO_3$ solution in the presence of the nacre protein Perlinhibin, an overgrowth of aragonite was found, possibly due to specific inhibition of calcite growth [59].

Hence, the possible roles of the crystal interacting proteins from the soluble matrix might be diverse, ranging from the control of crystal shape (growth inhibition or promotion of specific crystal faces) and polymorph selectivity (by specifically inhibiting calcite), to the general inhibition of uncontrolled growth from solution. For some of the proteins the attribute 'soluble matrix' may be misleading, since at least some of them are attached to the interlamellar matrix *in vivo* [158].

4.6. Crystallisation studies on the interlamellar matrix

In order to investigate the influence of the interlamellar matrix on mineral formation *in vitro*, a few crystallisation studies using water insoluble matrix extracts have been performed [156,180–182].

Greenfield et al. placed matrix sheets extracted with EDTA from septal nacre of *Nautilus pompilus* in metastable solutions with an ionic composition similar to the extrapallial fluid. Under these conditions, only a few crystals formed on the matrix. However, when matrix sheets with fixed soluble matrix proteins were used, a favoring of the crystallisation process was observed.[4] The authors concluded that soluble proteins are able to promote nucleation, when bound to the insoluble sheets [156]. This finding is in accordance with the study discussed earlier, of possible nucleating regions which require the use of protein fixating methods during demineralisation [23].

In a recent study, the authors remineralised the interlamellar matrix by using the ammonium carbonate gas diffusion method and simultaneous incubation with charged polymers (like poly-aspartic acid) which are known to stabilise amorphous calcium carbonate [181]. Electron micrographs of the resulting samples strongly resembled nacre's stacked mineral sheets and intercalated organic matrix; however, the polymorph formed was calcite. It is unclear whether the procedure used imitates processes *in vivo*, but obviously it supports the possibility of filling the organic compartments with crystalline matter by using stabilised ACC particles, which then subsequently transform to crystalline $CaCO_3$.

The common $CaCO_3$ crystallisation methods suffer from large deviations in pH value and concentration of the ions [183], which affects the rate of $CaCO_3$ precipitation as well as possibly important surface charges. These problems could be avoided by using a double diffusion method with constant renewal of the diffusing ionic solutions. When this method was used by Heinemann et al., crystallisation on the interlamellar matrix (demineralised by EDTA) resulted in the nucleation of flat aragonite crystal aggregates on and inside the interlamellar sheets (however, also unspecific crystals with the typical morphology for $CaCO_3$ precipitates were obtained). The specific crystals obtained resembled the aragonite tablets in nacre, whereas on several polymeric foils only the common morphologies of the water-free $CaCO_3$ polymorphs calcite, aragonite and vaterite were obtained. Thus, despite the aforementioned problems of EDTA demineralisation, as well as the possible loss of nucleating proteins, this

[3] The diffusion time was calculated by using $t = <r^2>/6D$. If the situation inside the organic matrix is considered as diffusion in a gel, an effective diffusion coefficient D_{eff} has to be calculated [174,175]. But due to the short distance r the resulting time t will remain small (<10 s), even under the assumption of strongly hindered diffusion ($D_{eff}/D = 0.01$).

[4] Although the crystal polymorph was not determined in the article, the needle-like morphology of the resulting crystals strongly resembled precipitated aragonite.

study showed the general capability of the EDTA demineralised interlamellar matrix to nucleate flat aragonite crystals *in vitro* [182].

5. Final remarks and future challenges

In this article we summarised our current view on structure, properties, and growth of gastropod nacre. With ongoing research and progress in scientific methods it became evident that these three aspects have to be considered in an integrated manner since they are tightly connected. For example, the discovery of structural details like the mineral bridges, the presence of correlated crystal axes over several platelets, or the heterogeneity of the chemical surface composition of the interlamellar matrix allowed to draw conclusions about the mechanism of growth. Also, macroscopic properties, like mechanical or optical characteristics, can only be understood in the light of a detailed structural understanding of nacre.

These mechanical and optical properties are features of nacre worth to imitate in biomimetic approaches. Inspired by the brick and mortar architecture at the micro-scale, artificial materials designed in a similar manner are promising approaches to obtain comparable fracture energies or optical properties. Since such artificial materials have a less restricted choice of ingredients, e.g. ceramics or engineered polymers, such materials may become even superior to their natural prototypes. However, the number of structural details, which are important for the properties are difficult to imitate in artificial multilayered composites. These details include the nanoasperities, the tablet waviness, the connection of the soft polymeric "mortar" with the hard ceramic "bricks" and the low thickness of the platelets. Additionally, so far the bio-inspired approaches for the production of nacre-like composites are time-consuming and laborious processes.

Therefore, a key feature of nacre biomineralisation, which would be highly promising to imitate in an artificial material, is its mechanism of growth. Such a material would possibly be self-growing in an aqueous solution and at ambient temperature. However, before biomimetic approaches are likely to succeed, which also imitate the growth process of nacre, a number of open questions needs to be solved. They can be grouped into questions related to the structure and composition, the assembly of the organic matrix, and the details of the calcium-carbonate crystallisation process.

Concerning the structure and composition a precise understanding of the configuration of the interlamellar matrix, including the lateral distribution of surface proteins and especially the arrangement and chemical nature of the putative nucleating regions on the interlamellar matrix is required. Moreover, it is still not conclusively known if, before mineralisation, the space between the interlamellar matrix sheets is filled with a proteinaceous gel, or if it can be considered as a relatively simple aqueous solution. In the case that such a gel exists before mineralisation, its fate during and after mineralisation would be highly interesting. For example, it could be either pushed away by the growing mineral or be included and form an intracrystalline network.

The second set of questions towards successful *in vitro* biomineralisation is a better understanding of the assembly of the interlamellar matrix in the extracellular space. Recent reports on amphiphilic properties of chitin purified from nacre suggest that this might drive at least partially the self-assembly of the interlamellar matrix. Further biochemical and structural characterisation of the chitin fraction as well as *in vitro* aggregation studies could provide more information here. Also, the recently published TEM images of vesicle like structures fusing with the surface of the developing interlamellar matrix point into an interesting direction.

Finally, crucial details of the crystallisation process resulting in the formation of oriented aragonite crystals with a defined morphology are unclear and represent obstacles to mimic this process. This is connected to a number of aforementioned unknown structural details of the organic matrix. For example, the ratio of free volume to nucleating surface in the extrapallial fluid during growth is not known, although this parameter is of great importance to the $CaCO_3$ nucleation process. Obviously the presence of a gel between the interlamellar sheets would greatly affect this ratio. Also, the detailed physical and chemical mechanisms of aragonite nucleation in nacre are still not clear (e.g., heteroepitaxy and ionotropy). A related question is the function and location of the soluble proteins *in vivo*. Some of these proteins seem to bind to the interlamellar matrix, where they possibly promote nucleation, whereas others might act as inhibitors in the volume. Furthermore, despite several indicators, a phase transition from amorphous calcium carbonate to a crystalline phase during adult nacre growth has not definitely been proven yet. Further crystallisation studies, ideally combined with physical modelling, might promote a better understanding of the influence of different organic fractions on the crystallisation process.

Acknowledgements

We thank Meike Gummich (Biophysics Institute, University Bremen) for helpful discussions and for providing the SDS-PAGE (sodium dodecylsulfate polyacrylamide gel electrophoresis) gel and we thank the referees of the manuscript for their valuable comments.

We thank Manfred Radmacher, head of the Biophysics Institute (Physics Department, University Bremen, Germany), for everyday helpful discussions and his continuous, generous support.

For his theoretical and practical expertise in electron microscopy, helpful discussions and his generous support, we thank Andreas Rosenauer (Electron Microscopy Group, Solid State Physics, Physics Department, University Bremen, Germany).

This work would not have been possible without the generous gift of abalone shells from Fred Glasbrenner (Australian Abalone Export Pty. Ltd., Laverton North, Victoria, Australia 3026).

We thank the DFG (Deutsche Forschungsgemeinschaft) (F.H., M.L., M.F.) and the University Bremen (K.G., M.F.) for their support.

References

[1] K. Wada, Crystal growth of molluscan shells, Bulletin of the National Pearl Research Laboratories 7 (1961) 703–828.
[2] H.K. Erben, On the structure and growth of the nacreous tablets in gastropods, Biomineralization 1 (1974) 14–27.
[3] H. Nakahara, An electron microscope study of the growing surface of nacre in two gastropode species *Turbo cornutus* and *Tegula pfeifferi*, Venus 38 (1979) 205–211.
[4] G. Bevelander, Abalone: Gross and Fine Structure, The Boxwood Press, Pacific Grove, 1988.
[5] H. Nakahara, G. Bevelander, M. Kakei, Electron microscopic and amino acid studies on the outer and inner shell layers of *Haliotis rufescens*, Venus 41 (1982) 33–46.
[6] A.P. Jackson, J.F.V. Vincent, R.M. Turner, The mechanical design of nacre, Proceedings of the Royal Society of London. Series B. Biological Sciences 234 (1988) 415–440.
[7] H.A. Lowenstam, Minerals formed by organisms, Science 211 (1981) 1126–1131.
[8] M. Snow, A. Pring, P. Self, D. Losic, J. Shapter, The origin of the color of pearls in iridescence from nano-composite structures of the nacre, American Mineralogist 89 (2004) 1353–1358.
[9] M. Meyers, P. Chen, A. Lin, Y. Seki, Biological materials: structure and mechanical properties, Progress in Materials Science 53 (2008) 1–206.
[10] Y. Dauphin, J.P. Cuif, H. Mutvei, A. Denis, Mineralogy, chemistry and ultrasructure of the external shell-layer in ten species of *Haliotis* with reference to *Haliotis tuberculata* (Molusca: Archaeogastropoda), Bulletin of the Geological Institute, University of Uppsala 15 (1989) 7–36.
[11] H. Espinosa, J. Rim, F. Barthelat, M. Buehler, Merger of structure and material in nacre and bone—perspectives on de novo biomimetic materials, Progress in Materials Science 54 (2009) 1059–1100.
[12] C.M. Zaremba, A.M. Belcher, M. Fritz, Y. Li, S. Mann, P.K. Hansma, D.E. Morse, J.S. Speck, G.D. Stucky, Critical transitions in the biofabrication of abalone shells and flat pearls, Chemistry of Materials 8 (1996) 679–690.
[13] A. Lin, M. Meyers, Growth and structure in abalone shell, Materials Science and Engineering A 390 (2005) 27–41.
[14] S. Wise, Microarchitecture and mode of formation of nacre (mother-of-pearl) in pelecypods, gastropods, and cephalopods, Eclogae Geologicae Helvetiae 63 (1970) 775–797.

[15] H. Nakahara, Calcification of gastropode nacre, in: P. Westbroeck, E.W. De Jong (Eds.), Biomineralization and Biological Metal Accumulation, D. Reidel Publishing Company, Dordrecht, Netherlands, 1983, pp. 225–230.
[16] H. Mukai, K. Saruwatari, H. Nagasawa, T. Kogure, Aragonite twinning in gastropod nacre, Journal of Crystal Growth 312 (2010) 3014–3019.
[17] M. Fritz, A.M. Belcher, M. Radmacher, D.A. Walters, P.K. Hansma, G.D. Stucky, D.E. Morse, S. Mann, Flat pearls from biofabrication of organized composites on inorganic substrates, Nature 371 (1994) 49–51.
[18] S. Weiner, L. Hood, Soluble protein of the organic matrix of mollusk shells: a potential template for shell formation, Science 190 (1975) 987–989.
[19] G. Falini, S. Albeck, S. Weiner, L. Addadi, Control of aragonite or calcite polymorphism by mollusk shell macromolecules, Science 271 (1996) 67–69.
[20] S. Mann, Biomineralization: Principles and Concepts in Bioinorganic Materials Chemistry, Oxford University Press, USA, 2001.
[21] T. Schäffer, C. Ionescu-Zanetti, R. Proksch, M. Fritz, D. Walters, N. Almqvist, C. Zaremba, A. Belcher, B. Smith, G. Stucky, Does abalone nacre form by heteroepitaxial nucleation or by growth through mineral bridges? Chemistry of Materials 9 (1997) 1731–1740.
[22] J. Bezares, R. Asaro, M. Hawley, Macromolecular structure of the organic framework of nacre in *Haliotis rufescens*: implications for growth and mechanical behavior, Journal of Structural Biology 163 (2008) 61–75.
[23] F. Nudelman, B. Gotliv, L. Addadi, S. Weiner, Mollusk shell formation: mapping the distribution of organic matrix components underlying a single aragonitic tablet in nacre, Journal of Structural Biology 153 (2006) 176–187.
[24] M. Rousseau, E. Lopez, P. Stempflé, M. Brendlé, L. Franke, A. Guette, R. Naslain, X. Bourrat, Multiscale structure of sheet nacre, Biomaterials 26 (2005) 6254–6262.
[25] A. Jackson, J. Vincent, R. Turner, Comparison of nacre with other ceramic composites, Journal of Materials Science 25 (1990) 3173–3178.
[26] H. Gao, B. Ji, I.L. Jäger, E. Arzt, P. Fratzl, Materials become insensitive to flaws at nanoscale: lessons from nature, Proceedings of the National Academy of Sciences of the United States of America 100 (2003) 5597–5600.
[27] S. Rama Swamy, X-ray analysis of the structure of iridescent shells, Proceedings Mathematical Sciences 2 (1935) 345–351.
[28] H. Mutvei, Ultrastructural characteristics of the nacre in some gastropods, Zoologica Scripta 7 (1978) 287–296.
[29] B. Bruet, H. Qi, M. Boyce, R. Panas, K. Tai, L. Frick, C. Ortiz, Nanoscale morphology and indentation of individual nacre tablets from the gastropod mollusc *Trochus niloticus*, Journal of Materials Research 20 (2005) 2400–2419.
[30] D. Chateigner, C. Hedegaard, H. Wenk, Mollusc shell microstructures and crystallographic textures, Journal of Structural Geology 22 (2000) 1723–1735.
[31] X. Li, W. Chang, Y. Chao, R. Wang, M. Chang, Nanoscale structural and mechanical characterization of a natural nanocomposite material: the shell of red abalone, Nano Letters 4 (2004) 613–617.
[32] K. Gries, R. Kröger, C. Kübel, M. Schowalter, M. Fritz, A. Rosenauer, Correlation of the orientation of stacked aragonite platelets in nacre and their connection via mineral bridges, Ultramicroscopy 109 (2009) 230–236.
[33] R. Wang, Z. Suo, A. Evans, N. Yao, I. Aksay, Deformation mechanisms in nacre, Journal of Materials Research 16 (2001) 2486.
[34] R. Ballarini, R. Kayacan, F.J. Ulm, T. Belytschko, A.H. Heuer, Biological structures mitigate catastrophic fracture through various strategies, International Journal of Fracture 135 (2005) 187–197.
[35] K. Gries, R. Kröger, C. Kübel, M. Fritz, A. Rosenauer, Investigations of voids in the aragonite platelets of nacre, Acta Biomaterialia 5 (2009) 3038–3044.
[36] R. Metzler, M. Abrecht, R. Olabisi, D. Ariosa, C. Johnson, B. Frazer, S. Coppersmith, P. Gilbert, Architecture of columnar nacre, and implications for its formation mechanism, Physical Review Letters 98 (2007) 268102.
[37] P. Gilbert, R. Metzler, D. Zhou, A. Scholl, A. Doran, A. Young, M. Kunz, N. Tamura, S. Coppersmith, Gradual ordering in red abalone nacre, Journal of the American Chemical Society 130 (2008) 17519–17527.
[38] R. Metzler, D. Zhou, M. Abrecht, J. Chiou, J. Guo, D. Ariosa, S. Coppersmith, P. Gilbert, Polarization-dependent imaging contrast in abalone shells, Physical Review B 77 (2008) 64110–64118.
[39] S. Blank, M. Arnoldi, S. Khoshnavaz, L. Treccani, M. Kuntz, K. Mann, G. Grathwohl, M. Fritz, The nacre protein perlucin nucleates growth of calcium carbonate crystals, Journal of Microscopy 212 (2003) 280–291.
[40] S. Weiner, Y. Talmon, W. Traub, Electron diffraction of mollusc shell organic matrices and their relationship to the mineral phase, International Journal of Biological Macromolecules 5 (1983) 325–328.
[41] S. Weiner, W. Traub, Macromolecules in mollusc shells and their functions in biomineralization [and discussion], Philosophical Transactions of the Royal Society of London. Series B, Biological Sciences 304 (1984) 425–434.
[42] I.M. Weiss, C. Renner, M.G. Strigl, M. Fritz, A simple and reliable method for the determination and localization of chitin in abalone nacre, Chemistry of Materials 14 (2002) 3252–3259.
[43] Ch. Jeuniaux, Chitine et Chitinolyse: un chapitre de la biologie moléculaire (Edited by Masson et Cie), 1963, pp. 127–135. Paris.
[44] G. Goffinet, Etude au microscope electronique de structures organisees des constituants de la conchioline de nacre du Nautilus macromphalus sowerby, Comparative Biochemistry and Physiology 29 (1969) 835–839.
[45] S. Weiner, W. Traub, X-ray diffraction study of the insoluble organic matrix of mollusk shells, Federation of European Biochemical Societies Letters 111 (1980) 311–316.
[46] F. Lucas, J. Shaw, S. Smith, Comparative studies of fibroins: I. The amino acid composition of various fibroins and its significance in relation to their crystal structure and taxonomy, Journal of Molecular Biology 2 (1960) 339–349.
[47] E. Degens, Molecular mechanisms on carbonate, phosphate, and silica deposition in the living cell, Topics in Current Chemistry 64 (1976) 1–112.
[48] J. Gosline, P. Guerette, C. Ortlepp, K. Savage, The mechanical design of spider silks: from fibroin sequence to mechanical function, Journal of Experimental Biology 202 (1999) 3295.
[49] S. Sudo, T. Fujikawa, T. Nagakura, T. Ohkubo, K. Sakaguchi, M. Tanaka, K. Nakashima, T. Takahashi, Structures of mollusc shell framework proteins, Nature 387 (1997) 563–564.
[50] B. Gotliv, L. Addadi, S. Weiner, Mollusk shell acidic proteins: in search of individual functions, ChemBioChem 4 (2003) 522–529.
[51] J. Evans, "Tuning in" to mollusk shell nacre- and prismatic-associated protein terminal sequences. Implications for biomineralization and the construction of high performance inorganic–organic composites, Chemical Reviews 108 (2008) 4455–4462.
[52] F. Marin, G. Luquet, Molluscan shell proteins, Comptes Rendus Palevol 3 (2004) 469–492.
[53] S. Weiner, Aspartic acid-rich proteins: major components of the soluble organic matrix of mollusk shells, Calcified Tissue International 29 (1979) 163–167.
[54] G. Fu, S. Valiyaveettil, B. Wopenka, D. Morse, $CaCO_3$ biomineralization: acidic 8-kDa proteins isolated from aragonitic abalone shell nacre can specifically modify calcite crystal morphology, Biomacromolecules 6 (2005) 1289–1298.
[55] F. Heinemann. Investigation of biopolymer–mineral interactions in the natural composite material nacre, PhD thesis Department of Physics, University of Bremen (2008).
[56] K. Mann, I. Weiss, S. Andre, H. Gabius, M. Fritz, The amino-acid sequence of the abalone (*Haliotis laevigata*) nacre protein perlucin, European Journal of Biochemistry 267 (2000) 5257–5264.
[57] I. Weiss, W. Göhring, M. Fritz, K. Mann, Perlustrin, a *Haliotis laevigata* (abalone) nacre protein, is homologous to the insulin-like growth factor binding protein N-terminal module of vertebrates, Biochemical and Biophysical Research Communications 285 (2001) 244–249.
[58] L. Treccani, K. Mann, F. Heinemann, M. Fritz, Perlwapin, an abalone nacre protein with three four-disulfide core (whey acidic protein) domains, inhibits the growth of calcium carbonate crystals, Biophysical Journal 91 (2006) 2601–2608.
[59] K. Mann, F. Siedler, L. Treccani, F. Heinemann, M. Fritz, Perlinhibin, a cysteine-, histidine-, and arginine-rich miniprotein from abalone (*Haliotis laevigata*) nacre, inhibits in vitro calcium carbonate crystallization, Biophysical Journal 93 (2007) 1246–1254.
[60] X. Shen, B.A. M., P.K. Hansma, G.D. Sucky, D.E. Morse, Molecular cloning and characterisation of lustrin A, a matrix protein from shell and pearl nacre of *Haliotis rufescens*. Journal of Biological Chemistry 272 (1997) 32472–32481.
[61] B.L. Smith, T.E. Schäffer, M. Viani, J.B. Thompson, N.A. Frederick, J. Kindt, A. Belcher, G.D. Stucky, D.E. Morse, P.K. Hansma, Molecular mechanistic origin of toughness of natural adhesives, fibres and composites, Nature 399 (1999) 761–763.
[62] M. Michenfelder, G. Fu, C. Lawrence, J. Weaver, B. Wustman, L. Taranto, J. Evans, D. Morse, Characterization of two molluscan crystal-modulating biomineralization proteins and identification of putative mineral binding domains, Biopolymers 70 (2003) 522–533.
[63] G. Fu, S. Qiu, C. Orme, D. Morse, J. De Yoreo, Acceleration of calcite kinetics by abalone nacre proteins, Advanced Materials 17 (2005) 2678–2683.
[64] F. Heinemann, M. Gummich, M. Radmacher, and M. Fritz. Modification of $CaCO_3$ precipitation rates by water-soluble nacre proteins, Materials Science and Engineering C (2010) doi:10.1016/j.msec.2010.08.005.
[65] L. Treccani, S. Khoshnavaz, S. Blank, K. vonRoden, U. Schulz, I. Weiss, K. Mann, M. Radmacher, M. Fritz, Biomineralizing proteins, with emphasis on invertebrate-mineralized structures, in: Fahnestock, Steinbüchl (Ed.), Biopolymers, Wiley-VCH Verlag GmbH, Weinheim, 2003, pp. 289–321.
[66] H. Ehrlich, P. Koutsoukos, K. Demadis, O. Pokrovsky, Principles of demineralization: modern strategies for the isolation of organic frameworks: part I. Common definitions and history, Micron 39 (2008) 1062–1091.
[67] H. Ehrlich, P. Koutsoukos, K. Demadis, O. Pokrovsky, Principles of demineralization: modern strategies for the isolation of organic frameworks: part II. Decalcification, Micron 40 (2009) 169–193.
[68] P. Gilbert, M. Abrecht, B. Frazer, The organic–mineral interface in biominerals, Reviews in Mineralogy and Geochemistry 59 (2005) 157.
[69] R. Metzler, I. Kim, K. Delak, J. Evans, D. Zhou, E. Beniash, F. Wilt, M. Abrecht, J. Chiou, J. Guo, Probing the organic–mineral interface at the molecular level in model biominerals, Langmuir 24 (2008) 2680–2687.
[70] A.H. Pfund, The colors of mother-of-pearl, Journal of Franklin Institute 183 (1917) 453–464.
[71] S. Kinoshita, S. Yoshioka, J. Miyazaki, Physics of structural colors, Reports on Progress in Physics 71 (2008) 1–30.
[72] Y. Liu, J.E. Shigley, K.N. Hurwitt, Iridescence color of a shell of the mollusk *Pinctada margaritifera* caused by diffraction, Optics Express 4 (1999) 177–182.
[73] T.L. Tan, D. Wong, P. Lee, Iridescence of a shell of mollusk *Haliotis glabra*, Optics Express 12 (2004) 4847–4854.
[74] D.J. Brink, N.G. van der Berg, An investigation of green iridescence on the mollusc *Patella granatina*, Journal of Physics D: Applied Physics 38 (2005) 338–343.
[75] S.M. Doucet, M.G. Meadows, Iridescence: a functional perspective, Journal of the Royal Society Interface 6 (2009) S115–S132.
[76] S.M. Porter, Seawater chemistry and early carbonate biomineralization, Science 316 (2007) 1302.
[77] A.Y. Zhuravlev, R.A. Wood, Eve of biomineralization: controls on skeletal mineralogy, Geology 36 (2008) 923–926.
[78] P.A. Sandberg, An oscillating trend in Phanerozoic non-skeletal carbonate mineralogy, Nature 305 (1983) 19–22.

[79] T.K. Lowenstein, M.N. Timofeeff, S.T. Brennan, L.A. Hardie, R.V. Demicco, Oscillations in Phanerozoic seawater chemistry: evidence from fluid inclusions, Science 294 (2001) 1086–1088.
[80] L.A. Hardie, Secular variation in seawater chemistry: an explanation for the coupled secular variation in the mineralogies of marine limestones and potash evaporites over the past 600 m.y. Geology 24 (1996) 279–283.
[81] J.B. Ries, Aragonite production in calcite seas: effect of seawater Mg/Ca ratio on the calcification and growth of the calcareous alga *Penicillus capitatus*, Paleobiology 31 (2005) 445–458.
[82] R.A. Berner, The role of magnesium in the crystal growth of calcite and aragonite from sea water, Geochimica et Cosmochimica Acta 39 (1975) 489–504.
[83] J.W. Morse, Q. Wang, M.Y. Tsio, Influences of temperature and Mg:Ca ratio on $CaCO_3$ precipitates from seawater, Geology 25 (1997) 85–87.
[84] L. Plummer, E. Busenberg, The solubilities of calcite, aragonite and vaterite in CO_2–H_2O solutions between 0 and 90 °C, and an evaluation of the aqueous model for the system $CaCO_3$–CO_2–H_2O, Geochimica et Cosmochimica Acta 46 (1982) 1011–1040.
[85] A. Gutjahr, H. Dabringhaus, R. Lacmann, Studies of the growth and dissolution kinetics of the $CaCO_3$ polymorphs calcite and aragonite I. Growth and dissolution rates in water, Journal of Crystal Growth 158 (1996) 296–309.
[86] J.W. Morse, R.S. Arvidson, The dissolution kinetics of major sedimentary carbonate minerals, Earth-Science Reviews 58 (2002) 51–84.
[87] A.G. Checa, C. Jiménez-López, A. Rodríguez-Navarro, J.P. Machado, Precipitation of aragonite by calcitic bivalves in Mg-enriched marine waters, Marine Biology 150 (2007) 819–827.
[88] J.G. Carter, E. Barrera, M.J. Tevesz, Thermal potentiation and mineralogical evolution in the Bivalvia (Mollusca), Journal of Paleontology 72 (1998) 991–1010.
[89] M.A. Crenshaw, The inorganic composition of molluscan extrapallial fluid, Biological Bulletin 143 (1972) 506–512.
[90] E.M. Harper, Are calcitic layers an effective adaptation against shell dissolution in the Bivalvia? Journal of Zoology 251 (2000) 179–186.
[91] P. Cubillas, S. Köhler, M. Prieto, C. Chaïrat, E.H. Oelkers, Experimental determination of the dissolution rates of calcite, aragonite, and bivalves, Chemical Geology 216 (2005) 59–77.
[92] S.A. Wainwright, Stress and design in bivalved mollusc shell, Nature 224 (1969) 777–779.
[93] M. Rubner, Synthetic sea shell, Nature 423 (2003) 925–926.
[94] L.J. Bonderer, A.R. Studart, L.J. Gauckler, Bioinspired design and assembly of platelet reinforced polymer films, Science 319 (2008) 1069–1073.
[95] E. Munch, M.E. Launey, D.H. Alsem, E. Saiz, A.P. Tomsia, R.O. Ritchie, Tough, bio-inspired hybrid materials, Science 322 (2008) 1516–1520.
[96] F. Barthelat, Nacre from mollusk shells: a model for high-performance structural materials, Bioinspiration & Biomimetics 5 (2010) 1–8.
[97] M.F. Ashby, Materials Selection in Mechanical Design, Pergamon Press Ltd., Oxford, 1992.
[98] U.G.K. Wegst, M.F. Ashby, The mechanical efficiency of natural materials, Philosophical Magazine 21 (2004) 2167–2181.
[99] M.H. Sadd, Elasticity — Theory, Applications, and Numerics, Academic Press, Burlington, MA, USA, 2009.
[100] A.I. Lurie, Theory of Elasticity, Springer-Verlag, Berlin, 2005.
[101] D. Gross, W. Hauger, J. Schröder, Technische Mechanik 2 — Elastostatik, Springer Verlag, Berlin, 2005.
[102] T.L. Anderson, Fracture Mechanics, Taylor & Francis, Boca Raton, 2005.
[103] J.G. Williams, Fracture mechanics of anisotropic materials, in: K. Friedrich (Ed.), Application of Fracture Mechanics to Composite Materials, Elsevier Science Publishers B.V., Amsterdam, 1989, pp. 3–38.
[104] M.E. Launey, On the Fracture Toughness of Advanced Materials, Lawrence Berkeley National Laboratory, 2009, Retrieved from http://www.escholarship.org/uc/item/7256s0nq on 19th of May 2009.
[105] J.D. Currey, J.D. Taylor, The mechanical behaviour of some molluscan hard tissues, Journal of Zoology 173 (1974) 395–406.
[106] J.D. Currey, Further studies on the mechanical properties of mollusc shell material, Journal of Zoology 180 (1976) 445–453.
[107] A.Y. Lin, M.A. Meyers, K.S. Vecchio, Mechanical properties and structure of *Strombus gigas*, *Tridacna gigas*, and *Haliotis rufescens* sea shells: a comparative study, Materials Science and Engineering C 26 (2006) 1380–1389.
[108] R. Rabiei, S. Bekah, F. Barthelat, Failure mode transition in nacre and bone-like materials, Acta Biomaterialia 6 (2010) 4081–4089.
[109] L. Liu, C. Chen, C. Lin, Y. Yang, Elasticity of single-crystal aragonite by Brillouin spectroscopy, Physics and Chemistry of Minerals 32 (2005) 97–102.
[110] C. Kearney, Z. Zhao, B.J.F. Bruet, R. Radovitzky, M.C. Boyce, C. Ortiz, Nanoscale anisotropic plastic deformation in single crystal aragonite, Physical Review Letters 96 (2006) 1–4.
[111] N.H. de Leeuw, S.C. Parker, Surface structure and morphology of calcium carbonate polymorphs calcite, aragonite and vaterite: an atomistic approach, Journal of Physical Chemistry B 102 (1998) 2914–2922.
[112] F. Barthelat, H.D. Espinosa, An experimental investigation of deformation and fracture of nacre — mother of pearl, Experimental Mechanics 47 (2007) 311–324.
[113] M.E. Broz, R.F. Cook, D.L. Whitney, Microhardness, toughness, and modulus of Mohs scale minerals, American Mineralogist 91 (2006) 135–142.
[114] M.A. Meyers, A.Y. Lin, P. Chen, J. Muyco, Mechanical strength of abalone nacre: role of the soft organic layer, Journal of the Mechanical Behavior of Biomedical Materials 1 (2008) 76–85.
[115] K.S. Katti, B. Mohanty, D.R. Katti, Nanomechanical properties of nacre, Journal of Materials Research 21 (2006) 1237–1242.
[116] H. Gao, B. Ji, M.J. Buehler, H. Yao, Flaw tolerant bulk and surface nanostructures of biological systems, Molecular and Cellular Biomechanics 1 (2004) 37–52.
[117] J.D. Currey, Mechanics of mother of pearl in tension, Proceedings of the Royal Society of London. Series B. Biological Sciences 196 (1977) 443–463.
[118] J. Cook, J.E. Gordon, C.C. Evans, D.M. Marsh, A mechanism for the control of crack propagation in all-brittle systems, Proceedings of the Royal Society of London. Series A. Mathematical and Physical Sciences 282 (1964) 508–520.
[119] G. Mayer, Rigid biological systems as models for synthetic composites, Science 310 (2005) 1144–1147.
[120] B. Ji, H. Gao, Mechanical properties of nanostructure of biological materials, Journal of the Mechanics and Physics of Solids 52 (2004) 1963–1990.
[121] R.M. McMeeking, A.G. Evans, Mechanics of transformation-toughening in brittle materials, Journal of the American Ceramic Society 65 (1982) 242–246.
[122] A.G. Evans, Z. Suo, R.Z. Wang, I.A. Aksay, M.Y. He, J.W. Hutchinson, Model for the robust mechanical behavior of nacre, Journal of Materials Research 16 (2001) 2475–2484.
[123] A.G. Evans, F.W. Zok, The physics and mechanics of fibre-reinforced brittle matrix composites, Journal of Materials Science 29 (1994) 3857–3896.
[124] J.C. McNulty, F.W. Zok, G.M. Genin, A.G. Evans, Notch-sensitivity of fiber-reinforced ceramic–matrix composites: effects of inelastic straining and volume-dependent strength, Journal of the American Ceramic Society 82 (1999) 1217–1228.
[125] F. Barthelat, C. Li, C. Comi, H. Espinosa, Mechanical properties of nacre constituents and their impact on mechanical performance, Journal of Materials Research 21 (2006) 1977–1986.
[126] F. Barthelat, H. Tang, P.D. Zavattieri, C.-M. Li, H.D. Espinosa, On the mechanics of mother-of-pearl: a key feature in the material hierarchical structure, Journal of the Mechanics and Physics of Solids 55 (2007) 306–337.
[127] K.S. Katti, D.R. Katti, S.M. Pradhan, A. Bhosle, Platelet interlocks are the key to toughness and strenght in nacre, Journal of Materials Research 20 (2005) 1097–1100.
[128] R. Menig, M.H. Meyers, M.A. Meyers, K.S. Vecchio, Quasi-static and dynamic mechanical response of *Haliotis rufescens* (abalone) shells, Acta Materialia 48 (2000) 2383–2398.
[129] J.H.E. Cartwright, A.G. Checa, The dynamics of nacre self-assembly, Journal of The Royal Society Interface 4 (2007) 491–504.
[130] S. Wise Jr., W. Hay, Scanning electron microscopy of molluscan shell ultrastructures II. Observations of growth surfaces, Transactions of the American Microscopical Society 87 (1968) 419–430.
[131] S. Wise Jr., Microarchitecture and deposition of gastropod nacre, Science 167 (1970) 1486.
[132] G. Bevelander, H. Nakahara, An electron microscope study of the formation of the nacreous layer in the shell of certain bivalve molluscs, Calcified Tissue International 3 (1969) 84–92.
[133] H. Nakahara, Nacre formation in bivalve and gastropod molluscs, Mechanisms and Phylogeny of Mineralization in Biological Systems, 1991, pp. 343–350.
[134] W. Schmidt, Studien über Pinnaperlen. I. Mitteilung: Über Prismenperlen von Pinna nobilis, Zoomorphology 25 (1932) 235–277.
[135] C. Gregoire, Topography of the organic components in mother-of-pearl, Journal of Cell Biology 3 (1957) 797.
[136] K. Towe, G. Hamilton, Ultrastructure and inferred calcification of the mature and developing nacre in bivalve mollusks, Calcified Tissue International 1 (1967) 306–318.
[137] H. Erben, N. Watabe, Crystal formation and growth in bivalve nacre, Nature 248 (1974) 2.
[138] L. Addadi, S. Weiner, Interactions between acidic proteins and crystals: stereochemical requirements in biomineralization, Proceedings of the National Academy of Sciences USA 82 (1985) 4110–4114.
[139] K. Wada, Studies on the mineralization of the calcified tissue in molluscs—X. Histochemical determination of the nature of acid mucopolysaccharide in organic crystals, Bulletin of the Japanese Society of Scientific Fisheries 30 (1964) 993–998.
[140] A. Lin, P. Chen, M. Meyers, The growth of nacre in the abalone shell, Acta Biomaterialia 4 (2008) 131–138.
[141] K. Wada, T. Fujinuki, Biomineralization in bivalve molluscs with emphasis on the chemical composition of the extrapallial fluid, The Mechanisms of Mineralization in the Invertebrates and Plants, 1976, pp. 175–190.
[142] C. Little, Ionic regulation in the queen conch, *Strombus gigas* (Gastropoda, Prosobranchia), Journal of Experimental Biology 46 (1967) 459.
[143] Y. Kitano, N. Kanamori, S. Yoshioka, Influence of chemical species on the crystal type of calcium carbonate, The Mechanisms of Mineralization in the Invertebrates and Plants, 1976.
[144] K. Wilbur, A. Bernhardt, Effects of amino acids, magnesium, and molluscan extrapallial fluid on crystallization of calcium carbonate: in vitro experiments, The Biological Bulletin 166 (1984) 251.
[145] F. Song, X. Zhang, Y. Bai, Microstructure and characteristics in the organic matrix layers of nacre, Journal of Materials Research 17 (2002) 1567–1570.
[146] R.A. Metzler, M. Abrecht, R.M. Olabisi, D. Ariosa, C.J. Johnson, B.H. Frazer, S.N. Coppersmith, P. Gilbert, Architecture of columnar nacre, and implications for its formation mechanism, Physical Review Letters 98 (2007) 268102–268105.
[147] K. Saruwatari, T. Matsui, H. Mukai, H. Nagasawa, T. Kogure, Nucleation and growth of aragonite crystals at the growth front of nacres in pearl oyster, *Pinctada fucata*, Biomaterials 30 (2009) 3028–3034.
[148] I. Weiss, V. Schönitzer, N. Eichner, M. Sumper, The chitin synthase involved in marine bivalve mollusk shell formation contains a myosin domain, FEBS Letters 580 (2006) 1846–1852.

[149] I. Weiss, S. Kaufmann, B. Heiland, M. Tanaka, Covalent modification of chitin with silk-derivatives acts as an amphiphilic self-organizing template in nacre biomineralisation, Journal of Structural Biology 167 (2009) 68–75.
[150] Y. Levi-Kalisman, G. Falini, L. Addadi, S. Weiner, Structure of the nacreous organic matrix of a bivalve mollusk shell examined in the hydrated state using cryo-TEM, Journal of Structural Biology 135 (2001) 8–17.
[151] L. Pereira-Mouries, M. Almeida, C. Ribeiro, J. Peduzzi, M. Barthelemy, C. Milet, E. Lopez, Soluble silk-like organic matrix in the nacreous layer of the bivalve *Pinctada maxima*, European Journal of Biochemistry 269 (2002) 4994–5003.
[152] L. Addadi, D. Joester, F. Nudelman, S. Weiner, Mollusk shell formation: a source of new concepts for understanding biomineralization processes, Chemistry - A European Journal 12 (2006) 980–987.
[153] F. Nudelman, E. Shimoni, E. Klein, M. Rousseau, X. Bourrat, E. Lopez, L. Addadi, S. Weiner, Forming nacreous layer of the shells of the bivalves *Atrina rigida* and *Pinctada margaritifera*: an environmental- and cryo-scanning electron microscopy study, Journal of Structural Biology 162 (2008) 290–300.
[154] A. Checa, J. Cartwright, M. Willinger, The key role of the surface membrane in why gastropod nacre grows in towers, Proceedings of the National Academy of Sciences 106 (2009) 38.
[155] M. Crenshaw, The soluble matrix from *Mercenaria mercenaria* shell, Biomineralization 6 (1972) 6–11.
[156] E. Greenfield, D. Wilson, M. Crenshaw, Ionotropic nucleation of calcium carbonate by molluscan matrix, Integrative and American Zoology 24 (1984) 925–932.
[157] A. Wheeler, J. George, C. Evans, Control of calcium carbonate nucleation and crystal growth by soluble matrix of oyster shell, Science (New York, NY) 212 (1981) 1397–1398.
[158] M. Crenshaw, H. Ristedt, The histochemical localization of reactive groups in septal nacre from *Nautilus pompilius* L, The Mechanisms of Mineralization in the Invertebrates and Plants, University of South Carolina Press, Columbia, SC, 1976, pp. 355–367.
[159] H. Thiele, A. Awad, Nucleation and oriented crystallization apatite in ionotropic gels, Journal of Biomedical Materials Research 3 (1969) 431–442.
[160] M.A. Crenshaw, H. Ristedt, Histochemical and structural study of nautiloid septa nacre, Biomineralization 8 (1975) 1–8.
[161] A. Wheeler, K. Rusenko, J. George, C. Sikes, Evaluation of calcium binding by molluscan shell organic matrix and its relevance to biomineralization, Comparative Biochemistry and Physiology Part B: Biochemistry and Molecular Biology 87 (1987) 953–960.
[162] S. Albeck, S. Weiner, L. Addadi, Polysaccharides of intracrystalline glycoproteins modulate calcite crystal growth in vitro, Chemistry - A European Journal 2 (1996) 278–284.
[163] L. Addadi, J. Moradian, N. Shay, S. Weiner, A chemical model for the cooperation of sulfates and carboxylates in calcite crystal nucleation: relevance to biomineralization, Proceedings of the National Academy of Sciences USA 84 (1987) 2732–2736.
[164] S. Mann, Molecular recognition in biomineralization, Nature 332 (1988) 119–124.
[165] L. Addadi, S. Raz, S. Weiner, Taking advantage of disorder: amorphous calcium carbonate and its roles in biomineralization, Advanced Materials 15 (2003) 959–970.
[166] S. Weiner, Y. Levi-Kalisman, S. Raz, L. Addadi, Biologically formed amorphous calcium carbonate, Connective Tissue Research 44 (2003) 214–218.
[167] A. Navrotsky, Energetic clues to pathways to biomineralization: precursors, clusters, and nanoparticles, Proceedings of the National Academy of Sciences of the United States of America 101 (2004) 12096.
[168] S. Weiner, I. Sagi, L. Addadi, Choosing the crystallization path less traveled, Science (Washington) 309 (2005) 1027–1028.
[169] B. Hasse, H. Ehrenberg, J. Marxen, W. Becker, M. Epple, Calcium carbonate modifications in the mineralized shell of the freshwater snail *Biomphalaria glabrata*, Chemistry European Journal, Weinheim 6 (2000) 3679–3685.
[170] J.C. Marxen, W. Becker, D. Finke, B. Hasse, M. Epple, Early mineralization in *Biomphalaria glabrata*: microscopic and structural results, Journal of Molluscan Studies 69 (2003) 113.
[171] I. Weiss, N. Tuross, L. Addadi, S. Weiner, Mollusc larval shell formation: amorphous calcium carbonate is a precursor phase for aragonite, Journal of Experimental Zoology 293 (2002) 478–491.
[172] R. Van Santen, The Ostwald step rule, The Journal of Physical Chemistry 88 (1984) 5768–5769.
[173] Y. Li, S. Gregory, Diffusion of ions in sea water and in deep-sea sediments, Geochimica et Cosmochimica Acta 38 (1974) 703–714.
[174] M. Lauffer, Theory of diffusion in gels, Biophysical Journal 1 (1961) 205–213.
[175] E. Johnson, D. Berk, R. Jain, W. Deen, Hindered diffusion in agarose gels: test of effective medium model, Biophysical Journal 70 (1996) 1017–1023.
[176] I. Weiss, S. Kaufmann, K. Mann, M. Fritz, Purification and characterization of perlucin and perlustrin, two new proteins from the shell of the mollusc *Haliotis laevigata*, Biochemical and Biophysical Research Communications 267 (2000) 17–21.
[177] S. Elhadj, J. De Yoreo, J. Hoyer, P. Dove, Role of molecular charge and hydrophilicity in regulating the kinetics of crystal growth, Proceedings of the National Academy of Sciences 103 (2006) 19237.
[178] A. Belcher, X. Wu, R. Christensen, P. Hansma, G. Stucky, D. Morse, Control of crystal phase switching and orientation by soluble mollusc-shell proteins, Nature 391 (1996) 56–58.
[179] J. Thompson, G. Paloczi, J. Kindt, M. Michenfelder, B. Smith, G. Stucky, D. Morse, P. Hansma, Direct observation of the transition from calcite to aragonite growth as induced by abalone shell proteins, Biophysical Journal 79 (2000) 3307–3312.
[180] G. Falini, S. Fermani, A. Ripamonti, Crystallization of calcium carbonate salts into beta-chitin scaffold, Journal of inorganic biochemistry 91 (2002) 475–480.
[181] N. Gehrke, N. Nassif, N. Pinna, M. Antonietti, H. Gupta, H. Cölfen, Retrosynthesis of nacre via amorphous precursor particles, Chemistry of Materials 17 (2005) 6514–6516.
[182] F. Heinemann, L. Treccani, M. Fritz, Abalone nacre insoluble matrix induces growth of flat and oriented aragonite crystals, Biochemical and Biophysical Research Communications 344 (2006) 45–49.
[183] A. Becker, M. Epple, A High-throughput Crystallization Device to Study Biomineralization In Vitro, Materials Research Society, Warrendale, Pa, 2005, p. 190.
[184] A.C. Maloof, D.P. Schrag, J.L. Crowley, S.A. Bowring, An expanded record of Early Cambrian carbon cycling from the Anti-Atlas Margin, Morocco, Canadian, Journal of Earth Science 42 (2005) 2195–2216.
[185] B. Bjellqvist, G. Hughes, C. Pasquali, N. Paquet, F. Ravier, J. Sanchez, S. Frutiger, D. Hochstrasser, The focusing positions of polypeptides in immobilized pH gradients can be predicted from their amino acid sequences, Electrophoresis 14 (1993) 1023–1031.
[186] M. Sarikaya, K.E. Gunnison, M. Yasrebi, I.A. Aksay, Mechanical property–microstructural relationships in abalone shell, Materials Research Society Symposium Proceedings 174 (1990) 109–116.
[187] Y. Sugimura, J. Meyer, M.Y. He, H. Bart-Smith, J. Grenstedt, A.G. Evans, On the Mechanical Performance of Closed Al Alloy Foams, Acta materialia 45 (1997) 5245–5259.
[188] W. Weibull, A Statistical Distribution Function of Wide Applicability, Journal of Applied Mechanics 18 (1951) 293–297.